DESIGN AND DEVELOPMENT OF A NOVEL DEVICE FOR THE UNIAXIAL MECHANICAL ANALYSIS OF CEREBRAL ARTERY TISSUE

by

Christen McPhee Hydrean

BS in Mechanical Engineering, University of Pittsburgh, 2007

Submitted to the Graduate Faculty of

The Swanson School of Engineering in partial fulfillment

of the requirements for the degree of

Master of Science in Mechanical Engineering

University of Pittsburgh

2009

UNIVERSITY OF PITTSBURGH

SWANSON SCHOOL OF ENGINEERING

This thesis was presented

by

Christen Hydrean

It was defended on

June 18, 2009

and approved by

Dr. Jeffery S. Vipperman, Associate Professor, Department of Mechanical Engineering and Materials Science

Dr. Lisa M. Weiland, Assistant Professor, Department of Mechanical Engineering and Material Science

Dr. William S. Slaughter, Associate Professor, Department of Mechanical Engineering and Material Science

Thesis Advisor: Dr. Anne M. Robertson, Associate Professor, Department of Mechanical Engineering and Material Science

DESIGN AND DEVELOPMENT OF A NOVEL DEVICE FOR THE UNIAXIAL MECHANICAL ANALYSIS OF CEREBRAL ARTERY TISSUE

Christen M. Hydrean, M.S.

University of Pittsburgh, 2009

In order to further advance the research of cerebral aneurysms, the study of the mechanical and structural properties of the cerebral arterial wall has been undertaken. A device has been designed and built that is capable of performing controlled uniaxial loading tests on arterial ring segments. The ring segments are placed around two carbon steel half-circle pins and then stretched to desired strains using a slide micrometer and stepper motor. During testing, the sample is immersed in a cuvette of saline solution to imitate in-vivo conditions. The load is measured using a load cell attached to the micrometer and the system is automated using Labview software. Strain can be determined from recorded images of the displacement of markers on the tissue or more roughly approximated by the pin displacement. To validate the device, studies were performed on fresh and frozen bovine carotid arteries.

Additionally, the device can be used to fix ring segments under prescribed loads or strain. In these applications, the tissue is loaded in the device and then fixed by filling the cuvette with paraformaldehyde solution. Upon removal from the solution, the internal elastic laminae (IEL) in the arterial segment is inspected and photographed under a confocal microscope to evaluate the fenestrae (natural holes) in the IEL as well as possible damage to the IEL. Past studies have revealed that elastin content and organization may be a key determinant in the intrinsic elastic properties of the arterial wall at low loads. The loss of the elastin membrane in cerebral arteries

is a distinguishing feature of early stage aneurysm formation. The device was used for preliminary studies of the effect of high strain on the IEL of human cerebral arteries. Large tears parallel to the direction of the folds in the IEL and perpendicular to the loading direction were observed. We conjecture that this failure mode may be important in transluminal angioplasty of cerebral vessels.

TABLE OF CONTENTS

LIST OF TABLES

LIST OF FIGURES

PREFACE

I would like to acknowledge my professor and advisor, Dr. Anne Robertson, for her guidance and support of this thesis project, as well as PhD. Candidate Michael Hill for his help and knowledge. Also, thank you to Dr. Rachimdian Wulandana and Andrew Holmes for their assistance through my thesis work.

1.0 INTRODUCTION

This research focuses on the coupling between mechanical and histological properties of the cerebral artery wall with respect to the development of human cerebral aneurysms. To explore this coupling, a uniaxial testing device was designed and built. It was then used for preliminary studies of human cerebral arteries.

1.1 CEREBRAL ANEURYSMS AND THE ARTERIAL WALL

A cerebral aneurysm is a bulging or weakened portion of an artery that arises from a pathological degeneration of the arterial wall. Aneurysms occur in approximately one percent of the population. (Tarren, 1965). Typically, an aneurysm causes no clinical symptoms until it leaks or catastrophically ruptures. At this point, the aneurysm can cause significant complications and blood loss or even death. Unfortunately, approximately 90% of patients are unaware of an aneurysm until they experience a severe headache caused by a leak or rupture of the aneurysm.

There are several types of cerebral aneurysms. The most common type, a saccular, or "berry" aneurysm is commonly found at bifurcation points in the cerebral vasculature. Bifurcation points are areas where arteries join together or split, causing a region of locally elevated wall shear stress and pressure near the vertex of the bifurcation. Aneurysms are most commonly found on or near a vasculature structure called the Circle of Willis, Figure 1.

The Circle of Willis is a meeting point of several large arteries that supply most of the blood to the brain. It is located at the base of the brain near the spinal cord. The circular geometry of the Circle of Willis is important because if one area of the circle becomes damaged or blocked, the other arteries can often compensate for the diminished flow in that region.

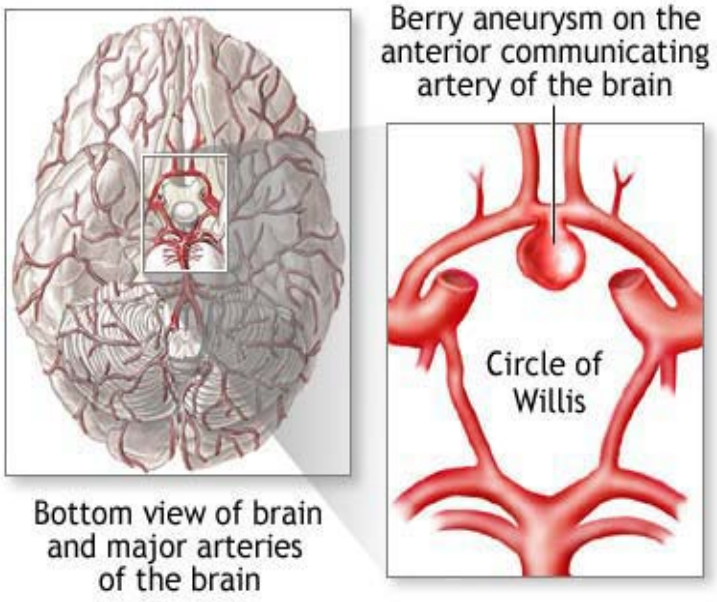

Figure 1: Circle of Willis and the occurrence of a saccular aneurysm (MD Consult, 2009)

The exact cause of cerebral aneurysms is still unknown. They occur in people of all ages and heath conditions. In many cases, the occurrence of an aneurysm is uncontrollable and unavoidable, since it stems only from the degeneration of the arterial wall. Variations from the ideal configurations of the Circle of Willis have been associated with a higher instance of aneurysms (Kayembe et al. 1984). The significance of asymmetry of the vessels in the circle of Willis, thickness of particular arteries and aneurysm location was investigated in 44 Circles of Willis. The variation from the "typical" circle of Willis was noted in each case, and a control

group of 148 circles without aneurysms was evaluated. The results from the study showed the incidence of variations in the circle of Willis with aneurysms was much higher than that for circles without aneurysms.

If detected, an aneurysm can be treated in two main ways. One approach is microvascular clipping, a process in which a surgeon inserts a small clothespin-like clamp on the aneurysm neck, restricting blood flow into the aneurysm sac. Another method is to implant a coil or balloon into the aneurysm sac to promote thrombosis. More recently, arterial stents have been used to diminish flow into the aneurysm sac. Stent placement has a significant influence on the hemodynamic flow within an aneurysm, and often more than one needs to be used to successfully occlude an aneurysm (Canton et al. 2005). Although these methods are effective, there is a great need to better understand the initiation, development and rupture process. Knowledge of this kind can be used to design better diagnostic and treatment strategies.

An important area of research is the development of constitutive theories that are capable of modeling the development of an aneurysm from a segment of arterial wall. A healthy artery wall is composed of three layers – the intima, media and adventitia, Figure 2. In extracerebral arteries, the three layers are separated by layers of elastin- a non-cellular highly elastic structural material. In cerebral arteries, only one elastin layer exists, located between the intima and media. This layer, called the internal elastic lamina (IEL), plays an intrinsic role in the mechanical properties of an artery. A second important structural material in the arterial wall is collagen.

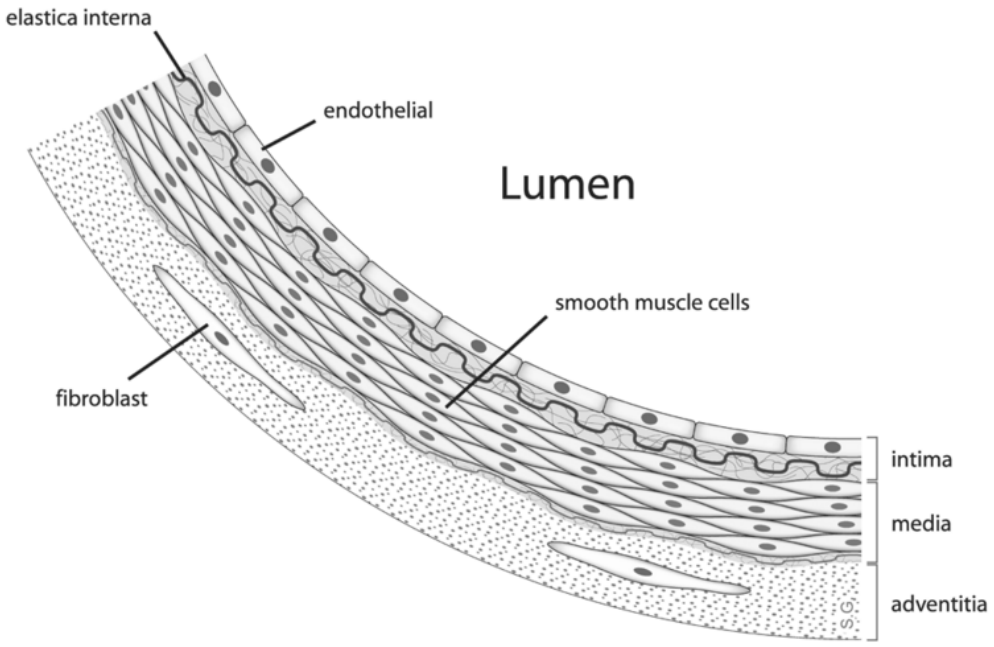

Figure 2: Cross-sectional view of cerebral artery wall

1.2 PREVIOUS RESEARCH ON CEREBRAL ANEURYSMS AND WALL MECHANICS

Research on cerebral aneurysms and the mechanical properties of arteries has been ongoing for decades. In 1971 researchers Scott, Ferguson and Roach, of the University of Western Ontario studied the elastic properties of human intracranial arteries and aneurysms (Scott et al. 1971). They discovered, through pressure-volume measurements of post-autopsy Circle of Willis arteries and aneurysms, that the mechanical behavior of the walls of cerebral arteries and aneurysms are significantly different. Aneurysms are much less distensible than

arteries. This is likely due to the lack of elastin in the aneurysm wall. The wall of a cerebral artery consists of an elastic lamella and collagenous tissue, whereas the wall of an aneurysm contains collagen and only fragments of elastin. (Hassler 1961, Nystrom, 1963). The thickness of the cerebral arteries and aneurysms also differ. A thickness of 100-200 microns was found for most cerebral arteries and thicknesses as low as 25microns were found for intracranial saccular aneurysms. The stress in an aneurysm is much higher because of this decreased thickness, along with the lack of elasticity and larger surface area. However, the specific load, pressure or strain required to achieve the formation of an aneurysm is still unknown. Studies have been performed to determine a growth rate of existing aneurysms as well. In a study by Allcock, et al. 82 aneurysms from 62 patients were investigated (Allcock et al. 1976). Angiograms of the aneurysms were taken at intervals ranging from days to 10 years. The study determined that the growth rate of aneurysms is not uniform among patients and individual aneurysms.

Scientists have not only studied the mechanical properties of cerebral arteries and aneurysms, but histological properties as well. In a study by Campbell et al. fenestration patterns in the internal elastic lamina were investigated (Campbell et al. 1984). Fenestrations are naturally occurring small holes in the elastic lamina. We conjecture that they may play a key role in the early stages of aneurysm formation. It has been shown that fenestrations are larger and more prevalent at bifurcation points in an artery. Campbell et al. also investigated the stretch of fenestrations in manually-fenestrated latex sheets. The sheets were perforated in both a random and grid configuration, in both normal and enlarged sizes. The solid latex sheets were loaded in uniaxial stretch at a speed of 100mm/min until 30% strain was achieved. Perforated sheets were tested in the same method, with the exception that the enlarged perforated sheets were stretched to 60%

strain to achieve the same load. The stress-strain relationship shows a significant difference between the sheets with larger fenestrations and the normally fenestrated and solid sheets.

Recently, a theoretical model has been developed that is capable of modeling damage to the IEL during loading (Wulandana and Robertson 2005, Li and Robertson 2009a, Li and Robertson 2009b). In this multi-mechanism model, elastin and collagen are modeled as separate entities with different unloaded reference configurations and material properties. In the earliest model, the damage to the IEL occurred in a discrete manner, arising when the strain exceed a specified criterion (Wulandana and Robertson 2005). More recently, this work was extended to include the anisotropic contribution of collagen as well as gradual damage to the IEL (Li, Robertson 2009 a, Li, Robertson 2009 b). In this model, the elastin degradation is considered as arising from two possible damage modes. In the first type, the degree of elastin degradation is a function of two local measures of strain: a maximum equivalent strain as well as an accumulated equivalent strain. In the second mode of damage, elastin degradation arises indirectly from hemodynamic loading. Motivation for this type of damage arises from animal studies which have shown that some combination of elevated hemodynamic loading leads to elastin degradation in native and non-native bifurcations (Morimoto 2002, Meng et al.2007, Gao et al. 2008). It seems likely that the abnormal hemodynamics initiate a cascade of biochemical activities that lead to degradation of the wall, rather than directly damaging the elastin. For example, some aspects of the hemodynamic loading may lead to an imbalance in the production of matrix metalloproteinases (MMPs) and tissue inhibitor of metalloproteinases **(**TIMPs) which break down the elastin in the IEL. Since cerebral aneurysms can form in humans in the absence of hypertension, we conjecture the role of elevated hemodynamic pressures in aneurysm formation is to hasten mechanical damage and ultimate failure of an elastin layer previously

weakened by biochemical factors. We expect the two damage mechanisms are coupled in aneurysm formation. For example, mechanical damage and ultimate failure can be hastened for an elastin layer previously weakened by biochemical factors. The damage model developed in (Li, Robertson, 2009 b) can also be used to study purely mechanical damage, as described in Eq. 1. In this model, the total contribution to the extra stress tensor arises from an isotropic contribution, $\underline{T}_{iso}$, (predominantly elastin) and an anisotropic contribution, $\underline{T}_{aniso}$ (the collagen contribution). Damage to the elastin mechanism is controlled through mechanical damage variables d_{01} and d_{02} as well as a hemodynamically derived damage variable d_{03}. The variable p in Eq. 1 epresents the Lagrange multiplier arising from an incompressibility restraint.

$$\begin{aligned}\underline{T} &= -p\underline{I} + \underline{T}_{iso} + \underline{T}_{aniso} \\ &= -p\underline{I} + (1-d_{01})(1-d_{02})(1-d_{03})\underline{T}_0 + \sum_{i=1}^{2}(1-d_i)\underline{T}_i \\ &= -p\underline{I} + 2(1-d_{01})(1-d_{02})(1-d_{03})\left(\frac{\partial \psi_0}{\partial I_0}\underline{B}_0\right) \\ &+ \sum_{i=1}^{2} 2(1-d_i)\left(\frac{\partial \psi_i}{\partial I_i}\underline{B}_i + \frac{\partial \psi_i}{\partial IV_{i,i}}\underline{F}_i \cdot \underline{a}_{i,i} \otimes \underline{F}_i \cdot \underline{a}_{i,i}\right),\end{aligned} \tag{1}$$

Such a model has recently been applied to the study of percutaneous transluminal angioplasty (PTA) (Li, Robertson, 2009 c). This procedure is sometimes performed in cerebral vessels to treat atherosclerotic obstruction and vasospasm. During this treatment, the vessel is inflated with a balloon to a larger diameter than its native value. Transluminal dilatation of small and fragile intracranial arteries is more dangerous than that of extracranial arteries and can induce direct vascular damage. A purely mechanical damage model is appropriate for these cases because it occurs over a time scale too short for a secondary response to hemodynamic loads to be important.

One of the central goals of this research is to determine the effects of large strain on the IEL including loading to the point of irreversible damage to the IEL. This information will be directly useful for the development of the mechanical damage aspects of this multi-mechanism constitutive equation (Li, Robertson, 2009 b). In particular, it will help to clarify the modes of purely mechanical damage under large strain. Uniaxial mechanical devices cannot be used to determine anisotropic mechanical properties of the artery wall. In the future, this device can be used in conjunction with histological studies to elucidate the anisotropic properties of the material.

2.0 DEVICE DESIGN – UNIAXIAL TESTING DEVICE

This chapter will discuss the design and development of a device for uniaxial testing of ring segments of arterial tissue and their subsequent fixation for histological studies. It will also detail the design of devices and histological experiments by previous researchers.

2.1 INITIAL GOALS AND DESIGN

2.1.1 Previous Histological Studies

In a study performed by Gonzalez et al. small sections of arteries from various aged rats were pressurized and fixed to determine elastin content and organization in the internal elastic lamina (Gonzalez et al. 2005). Briefly, the vessel was attached to two microcannulae and filled with an oxygenated calcium-free Krebs-Henesleit solution. The pressure was increased as the inner and outer diameters of the artery were measured until the internal pressure reached 70 mm Hg. The loaded vessel was submerged in paraformaldehyde solution to fix the proteins of the artery and under the given loading conditions. Afterwards, the arteries were viewed with a confocal microscope to evaluate the fenestrations. The study showed that older rats had more

fenestrations in the IEL than those of younger rats and cerebral arteries have the thinnest IEL to begin with.

It was determined that increased number and size of fenestrations in the IEL correlated with arterial stiffness, which in turn correlated with the occurrence of aneurysms. This study showed a correlation of pressure, age, artery location with IEL thickness and fenestration area. However, these results are for rats, which do not spontaneously form cerebral aneurysms. In this work, we study the effects of mechanical loading on the structure of the arterial wall in human cadaver arteries from the Circle of Willis.

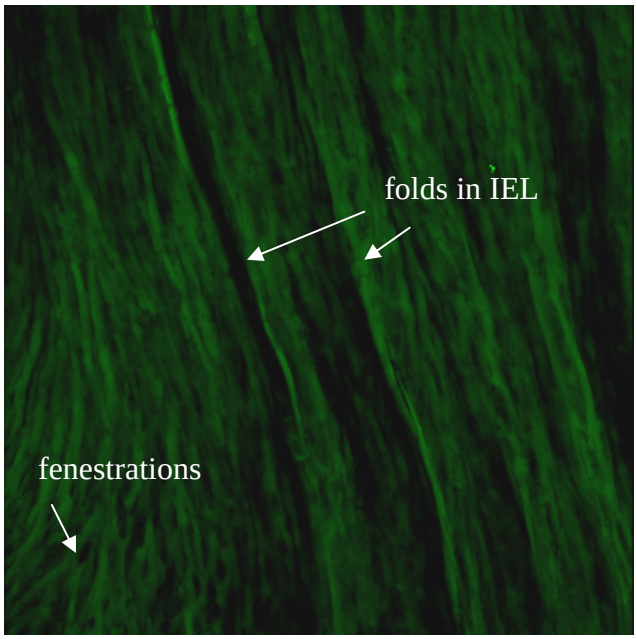

Figure 3: 20x confocal image of IEL in unstretched artery. Folds and small fenestrations are shown.

Although studies have also been done to research the influence of pressure on the IEL and arterial wall in humans, the images are difficult to evaluate because of the folds in the IEL. A representative figure of an unloaded artery is shown in Figure 3. The folds in the image interfere with clear viewing of the fenestrations. An early objective of this work was the design

of a device that would be able to stretch ring segments while immersed in a paraformaldehyde solution. Thereby, making it possible to fix the tissue in a configuration where the folds are opened up, enabling clear viewing of the fenestrae.

2.1.2 Previously designed uniaxial devices

Several researchers have developed uniaxial devices for biological tissue. However, many of these devices do not allow for the uniaxial study of an intact ring segment. One such device was created by researchers at Budapest University of Technology and Economics and Semmelweis University (Toth et al. 2005). Toth et al. created both uniaxial and biaxial devices for stretching strips of cerebral artery and aneurysm tissue. In this work, 110 strips of 3mm width were cut from aneurysms of 51 patients. To imitate "in vivo" conditions, they were insulated in a Krebs-Ringer solution at 37C and stretched to 200μm/2 minutes until tearing occurred. Strips were taken in both the circumferential direction and meridonal direction, in both thick and thin areas. The device used strain gages to measure displacement. The applied force was also measured. Aneurysm strips displayed the expected hyperelastic plastic behavior during these tests. It was also noted that thin strips in the meridional direction exhibited larger tensile strength than thick ones.

In this work, a device is designed to test ring segments rather than isolated strips of tissue. This choice was made because ring segments require less manipulation/cutting of the tissue. This manipulation can cause irreversible changes to the tissue and thereby invalidate the results. A disadvantage is that we must confine attention to circumferentially oriented segments. Furthermore uniaxial tests alone cannot provide information about the anisotropic nature of the vessel. However, this limitation can be addressed when histological studies of fiber orientation

are performed in conjunction with uniaxial experiments. Generally, the tissue sample size in biaxial tests must be larger than for ring segment studies. In fact, entire vessel segments are often used in biaxial experiments of arteries.

2.1.3 Goals of initial project and initial design

The initial goal of this project was to design a testing device that would uniaxially stretch a segment of arterial tissue immersed in a cuvette of liquid (either saline or paraformaldehyde). For applications to human vessels, the device should be able to hold an arterial ring segment approximately one centimeter wide (controlled by the pin length). The device should be able to stretch this segment to a prescribed length set by the user. After stretch, the device should be capable of holding the strain until the tissue is fixed in paraformaldehyde solution. Since the design uses paraformaldehyde, a known human carcinogen and mutagen, necessary precautions needed to be taken to ensure the device would be safe to use. The device also needed to be compatible with safety areas such as a fume hood. For this reason, a small footprint was necessary. Furthermore, the device needed to be portable for easy transport by a user between laboratories.

In the Fall of 2007, C. Hydrean, B. Young, and J. Barry, designed and built a mechanical device meeting these requirements for a senior design project at the University of Pittsburgh, Figs. 4 and 5 (Barry et al. 2007). This device uses a slide micrometer (Velmex slide micrometer, scale and veneer series A15) and stainless steel pin mechanism to stretch the tissue segments. The pin area is small enough to fit inside a cuvette of liquid held in the delrin base of the device.

A high speed camera is used to measure the distance between the two pins from a front-view position during a test, providing an estimate of tissue strain.

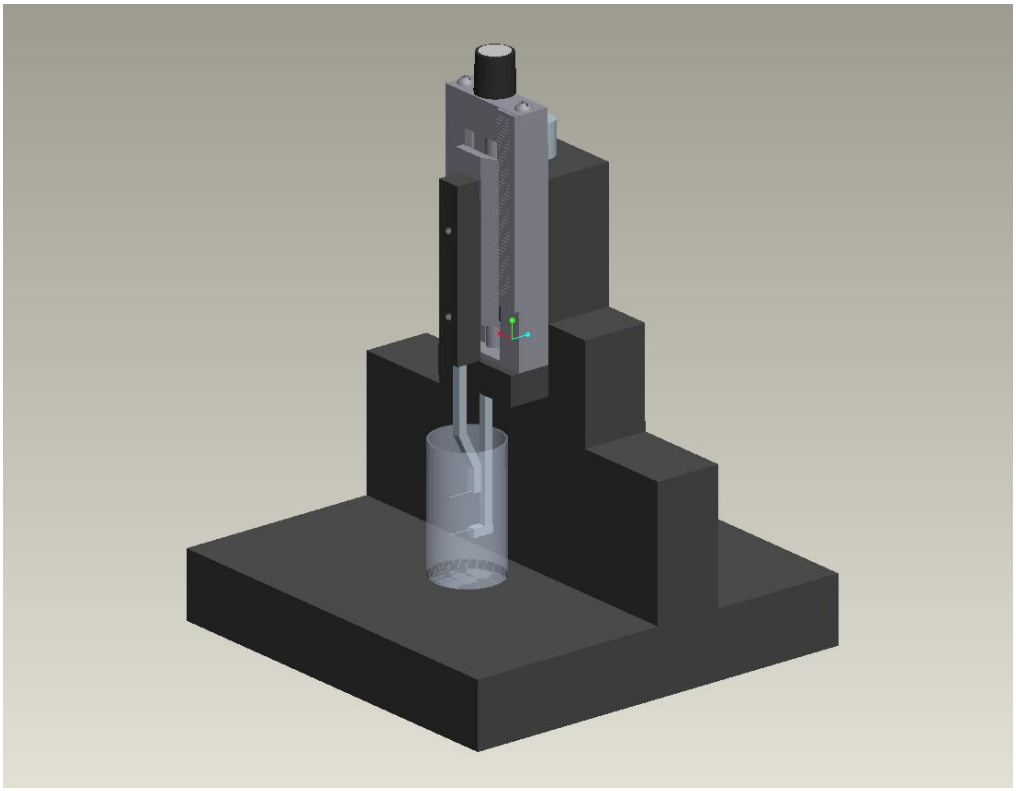

Figure 4: Initial device design for manual stretching and fixation of arterial ring segments

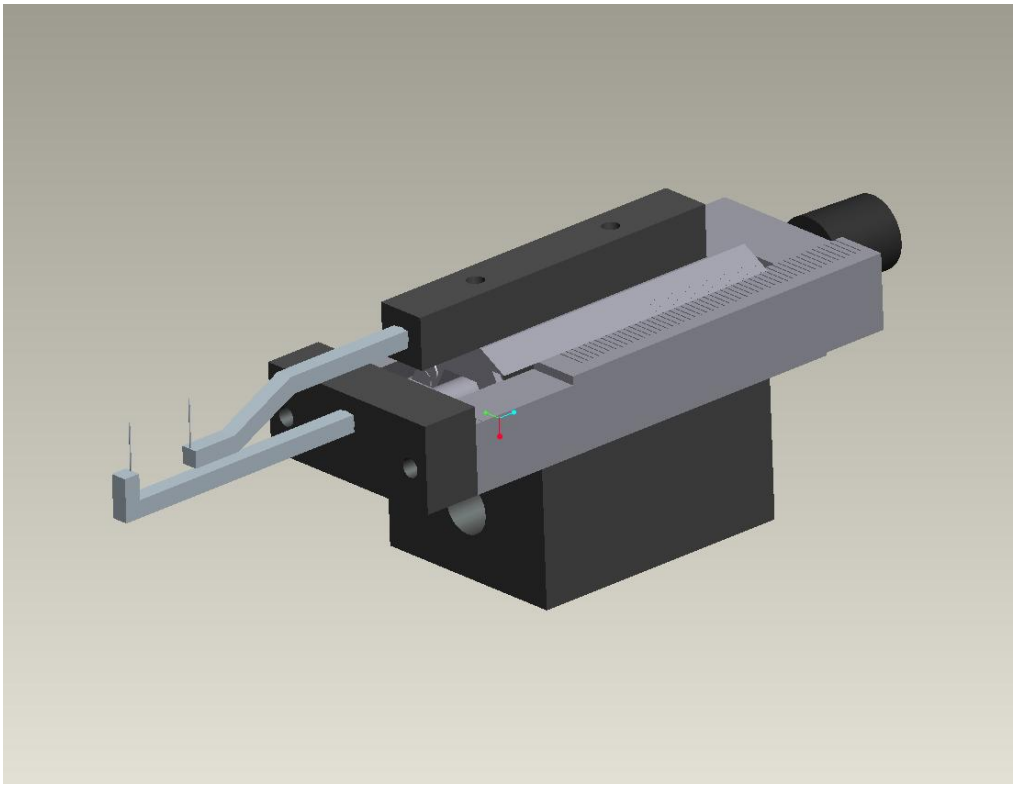

Figure 5: Detailed view of micrometer slide portion, showing pin mechanism.

At the beginning of this thesis work, this initial device was used to perform histological experiments on cerebral artery tissue. The histological results will be discussed in the following sections of the thesis.

2.2 DESIGN OF THE CURRENT DEVICE

After the first model of the device was made, changes were both desired and necessary. To evolve the device into a semi-automated system with data collection capability took many design changes and upgrades. Among the various design changes were the redesign of the pin

mechanism, incorporation of a load cell and motor control and automation. These changes allowed the research to progress in a more quantitative direction.

2.2.1 Pin Mechanism

The first design of the pin mechanism consisted of two stainless steel hypodermic needles mounted onto stainless steel rods. These needles were 0.025 inches in outer diameter. As the micrometer slide was turned, the top pin would move up or down depending on the direction chosen. Figure 6 shows this movement.

Figure 6: Graphical interpretation of initial pin mechanism. Blue cylinder represents artery segment. Green cylinders represent stainless steel pins.

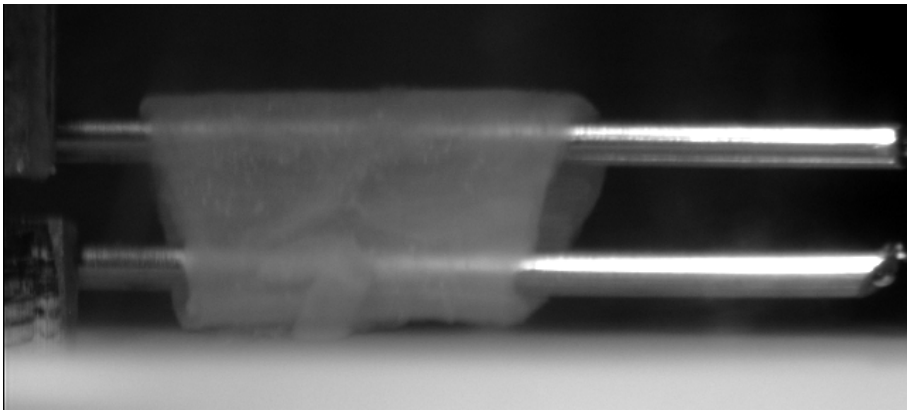

Figure 7: Photographed side view of initial pin mechanism and artery

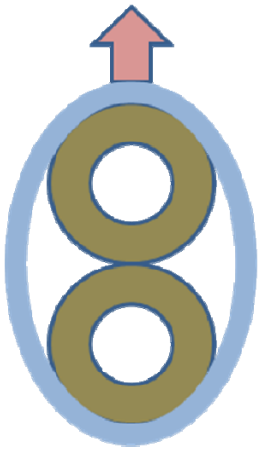

Figure 8: Graphical interpretation of initial pin mechanism with artery, front view.

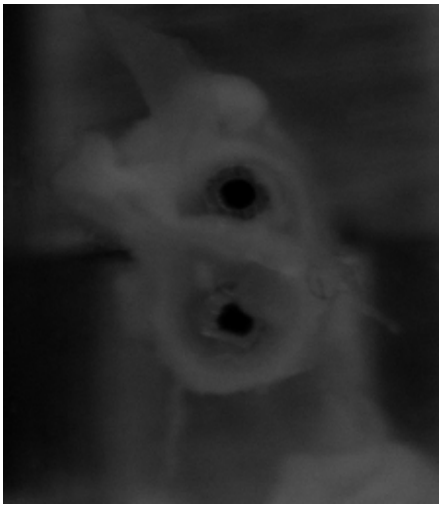

Figure 9: Photograph of front view of initial pin design

After initial testing on the device, it was determined that these pins needed to be redesigned. The small surface area of the pins damaged the arterial wall in some cases due to high stress concentrations. A more robust design was introduced, changing the cross sectional shape of the pins from full circle to half circles, Figs. 8-12. Larger diameters can be used to generate a greater surface contact area. These pins are machined from carbon steel and provide

a larger surface area for artery contact and therefore less damage is done to the artery upon stretching.

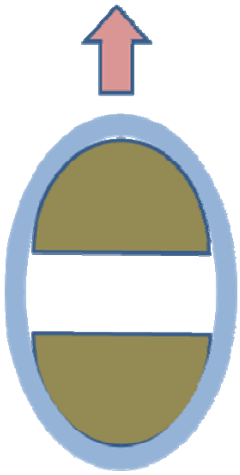

Figure 10: Graphical interpretation of new pin mechanism design, shown from front view.

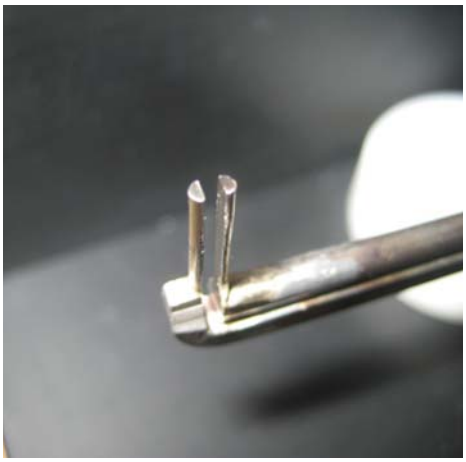

Figure 11: Photograph of new pin design.

Figure 12: Photographed Front view of revised pin design. Image taken in saline with cerebral artery attached

2.2.2 Load Cell

The initial design of this device was purely mechanical and manually controlled. In order to determine a correlation between strain and stress on the artery wall, a load cell was introduced. The device was re-designed to incorporate a tension and compression load cell. After several different design attempts and three different load cells, a final design was developed. The device incorporates a MDB Series Load Cell from Transducer Techniques. The active end of the load cell is directly attached to the moving pin of the device to most accurately measure force on the artery during movement. The body of the load cell is mounted on the micrometer slide. An image of the load cell is shown in Figure 14. The load cell was calibrated using a range of weights.

Figure 13: Load Cell Assembly

2.2.3 Controls – Motor and Automation

One of the most important aspects of determining a stress and strain relationship is precise control of the applied strain at a specified strain rate. Therefore, to automate the device and lessen human error, a stepper motor was introduced into the system. One full turn on the micrometer slide is equivalent to a displacement of 1 mm. In the high range of the stepper motor, speeds of 100 to 12,000 steps/second can be achieved. The low range of the motor can achieve speeds of 10 to 1,200 steps/second. Using a gear reducer, the motor can run at much lower speeds. The gear reducer equates 596.6 revolutions of the motor to one revolution of the micrometer slide, which is equal to 1 mm. Therefore, the motor and gear reducer can control the micrometer at speeds ranging from 8.38E-6 mm/s to 0.1mm/s. The motor is directly attached to

the micrometer slide, replacing the manual advancing knob. To control the motor, Labview software is used. The program achieves the desired displacement by how fast and how long the motor is moving.

In addition to the motor automation, a high definition camera can simultaneously record images of the pin mechanism at specified time intervals. The camera can also be run independently to measure artery dimensions. Figure 14 shows a schematic of motion and data transfer in an experiment. The motion is transferred from the motor to the pin mechanism to the artery segment, while the data is collected by the motor, load cell and camera for each respective leg of motion. Finally, the data is transferred from these three systems to the computer and Labview. An image of the complete test system is shown in Figure 15.

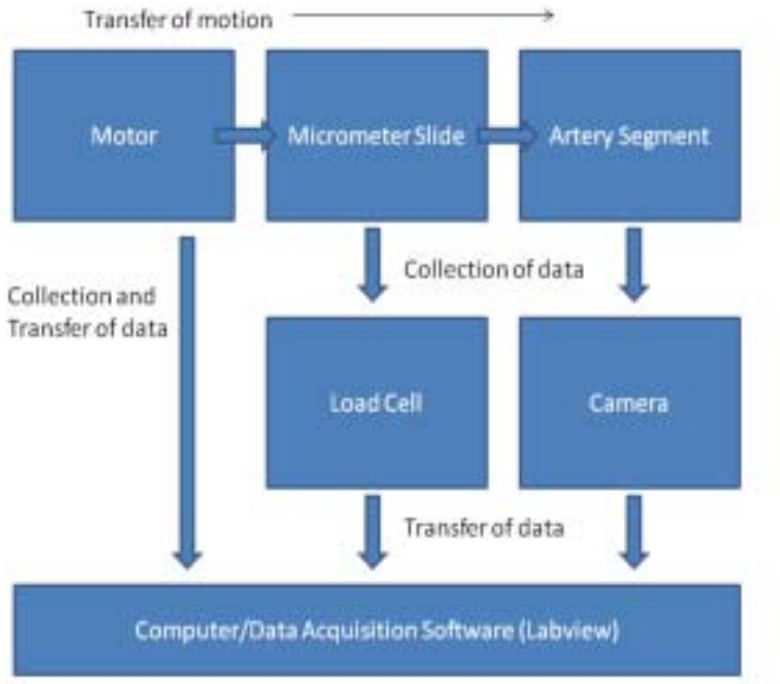

Figure 14: Schematic of Motion and Data Transfer

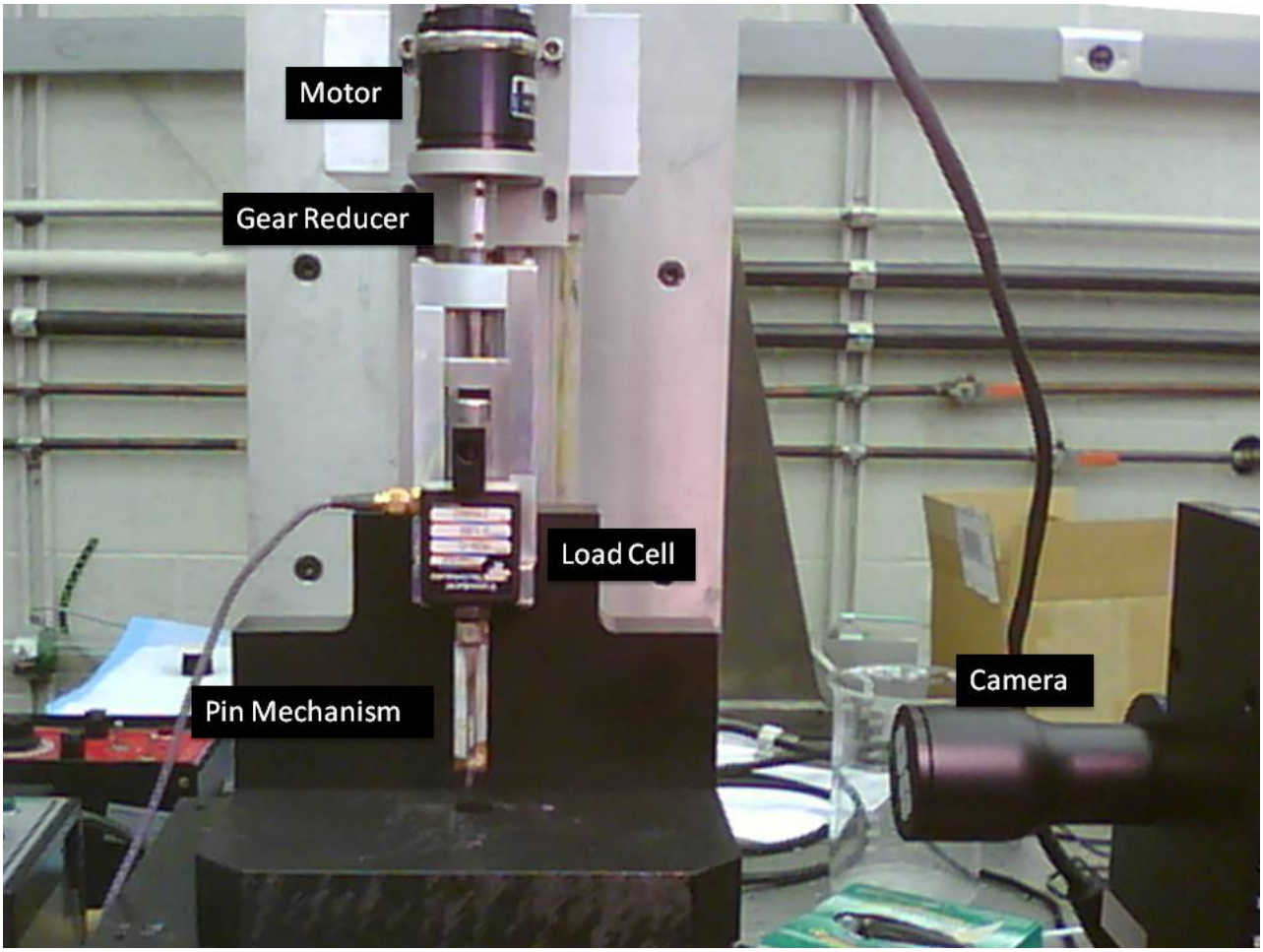

Figure 15: Photograph of entire testing system.

3.0 HISTOLOGY RESULTS

3.1.1 Histology Protocol

To determine the effects of high strains on the elastin organization in cerebral arteries, several tests were performed on previously frozen human cadaver arteries. Complete Circles of Willis, donated by Alzheimer's disease patients, were stored in a -80C freezer at the UPMC Brain Bank. The circles were retrieved from the UPMC Brain Bank and stored at approximately -30C in a freezer in the BioTissue and Complex Fluids Laboratory. The amount of time each artery was frozen differs, and is unknown. Each Circle of Willis has a serial number, which is used to distinguish one from another.

The previously mentioned study by Gonzalez et al. (2005) on the fenestrations in the IEL of rat arteries motivated the current study on human arteries. Using the protocols for paraformaldehyde fixation technique and confocal microscopy described in that work, the current study was designed to investigate the fenestrations in the IEL of human cerebral arteries under high strains. An earlier design of the device was used for this work. The pin mechanism had been redesigned, but no motor or load cell were used in this design. The following protocol was used for these tests:

1. Circle of Willis are thawed at room temperature for approximately 20 minutes.
2. A diagram of the artery is entered in the lab notebook, to keep track of what branches are used.
3. Two adjacent ring segments are cut from the desired artery using dissection scissors: one for strain testing and the other to serve as a control (unstrained).
4. The diameter, thickness and width of the samples are measured using calipers.
5. The control segment is placed in a cuvette of saline and set aside. Saline is used because of its similar osmolarity of NaCl to that of blood.
6. The ring segment to be strain fixed is placed on the pins of the uniaxial device and immersed in the saline within the cuvette.
7. In most cases, the inner circumference of the artery is larger than the surface area of the half-circle pins when touching, so starting pin distance, L_0, is designated as the point at which the artery touches the pins completely, Figure 16. This point is found using the camera, visualized from the front.

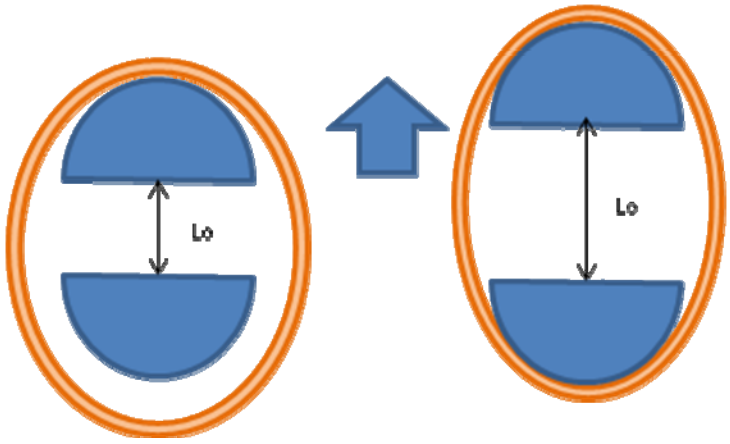

Figure 16: Diagram of L_0 protocol, also used for R_x

8. Each artery was stretched and released manually at least three times while immersed in saline before being fixed at the prescribed distance. Each stretch and release distance was recorded. Extension distances are designated as E_x. Release distances are determined the same way as L_0, and are designated as R_x.
9. After the desired number of extensions and releases, the artery is extended to the full desired strain and fixed with 4% paraformaldehyde solution for one hour. Paraformaldehyde solution fixes the proteins in the tissue, keeping the orientation of elastin fibers in the configuration experienced upon strain.
10. Post fixation in the paraformaldehyde solution, the artery segments are rinsed with a Phosphate Buffer Solution, cut axially and mounted on glass slides for microscopy, Figure 17.

Confocal microscopy was performed on an Olympus F500 microscope with FITC filtering. Elastin is fortunately autoflourescent, and appears green in all images. This makes fenestration area and size easy to interpret.

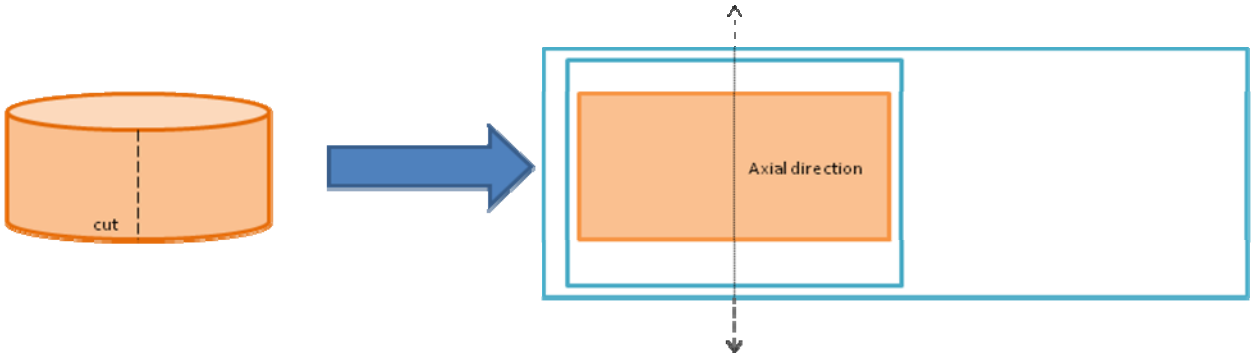

Figure 17: Arterial Ring Segment microscope mounting diagram.

3.1.2 Strain Data

Using the protocol above, several tests were performed to various strains. Table 1 shows the position data from one set of experiments. L_0 is the initial pin separation, E_1 through E_5 are the extension points and R_1 through R_5 are the relax/release points. The final point is where the artery was fixed in paraformaldehyde solution, and this value was used to determine total final applied strain from the beginning position. Strain was determined using Eq. 2.

$$\text{Strain} = (L-L_0)/L_0 \qquad (2)$$

It should be noted that engineering strain is used in this case, however it can be converted to true strain if desired. It is also assumed that the artery is in perfect contact with the pins. Additional idealizations and potential sources of error are discussed below. They include, for example, the error arising from the use of pin separation as a measure of strain. This error will increase with the level of the non-uniformity of the strain field.

Table 1: Raw data from each uniaxial strain experiment

	CW08-007 PCA	A08-125 MCA1	CW08-007 MCA	A08-125 ACA	CW07-008 MCA	A08-125 MCA2	CW08-006 MCA	CW07-008 PCA
L0(mm)	0.8539	1.32756	1.4662	0.4953	0.7964	0.53493	0.45611	0.09906
E1	1.3149	2.7538	2.8356	1.0698	1.7079	1.34737	2.19995	1.111
R1	0.974	2.23886	2.0606	0.79348	0.99	0.555	0.97261	0.19911
E2	1.27045	2.8265	3.112	1.5064	2	1.2686	2.63688	1.36833
R2	0.9345	2.41741	2.259	0.87174	1.21	0.75286	1.40666	0.57455
E3	1.30808	3.21055	3.725	1.18873	2.122	1.80302	2.91246	1.78486
R3	0.951	2.35773	3.1507	0.93117	1.19	0.971	1.4871	0.6541
E4	1.28916	3.1507	3.6262	1.24958	2.1653	1.82283	2.95627	2.02826
R4	na	2.49759	na	0.95098	na	1.24817	1.60918	na
E5	na	3.13031	na	1.16959	na	1.82272	3.07191	na
R5	na	2.51622	na	0.89243	na	1.06886	1.58807	na
final	1.28916	3.15169	3.6262	1.26813	2.1653	1.84349	3.0323	2.02826
final applied strain:	50.97%	137.40%	147.32%	156.03%	171.89%	244.62%	564.82%	1947.51%

From this table it can be deduced that the unloaded state of each artery increased with strain. The data has high variation due to the nature of the tests. The arteries were chosen to be stretched to a variety of different strains to investigate the histological effects through a range of distances. Figure 18 shows the increase in unloaded state graphically. It can be seen that the unloaded states increase with each stretch cycle, but tend to plateau after several cycles. In arteries CW08-006 MCA, A08-125 MCA1, and A08-125 ACA the increase is monotonic, but for the remainder of the arteries the increase is nonmonotonic. Figure 19 shows one complete experiment graphically for artery number CW08-006 MCA during a cyclic loading experiment to total of 564% strain. Figure 20 shows an example of camera images taken from an experiment. The tissue experienced visible tearing. However, the exact relaxation data would need to be analyzed with loading data and time control as well. The lack of loading rate control is an issue in this experiment. To keep results consistent, a slow and steady loading rate must be implemented. With the implementation of a consistent load rate and simultaneous load measurement, mechanical parameters such as yield strength may eventually be determined. These parameters can help customize the constitutive models for different types of arteries.

However, the data is not sufficient to achieve this currently. Due to the restrictions of the device in its early design, the error in reported strains may be significant due to human error in turning the micrometer and the end effects caused by the pins.

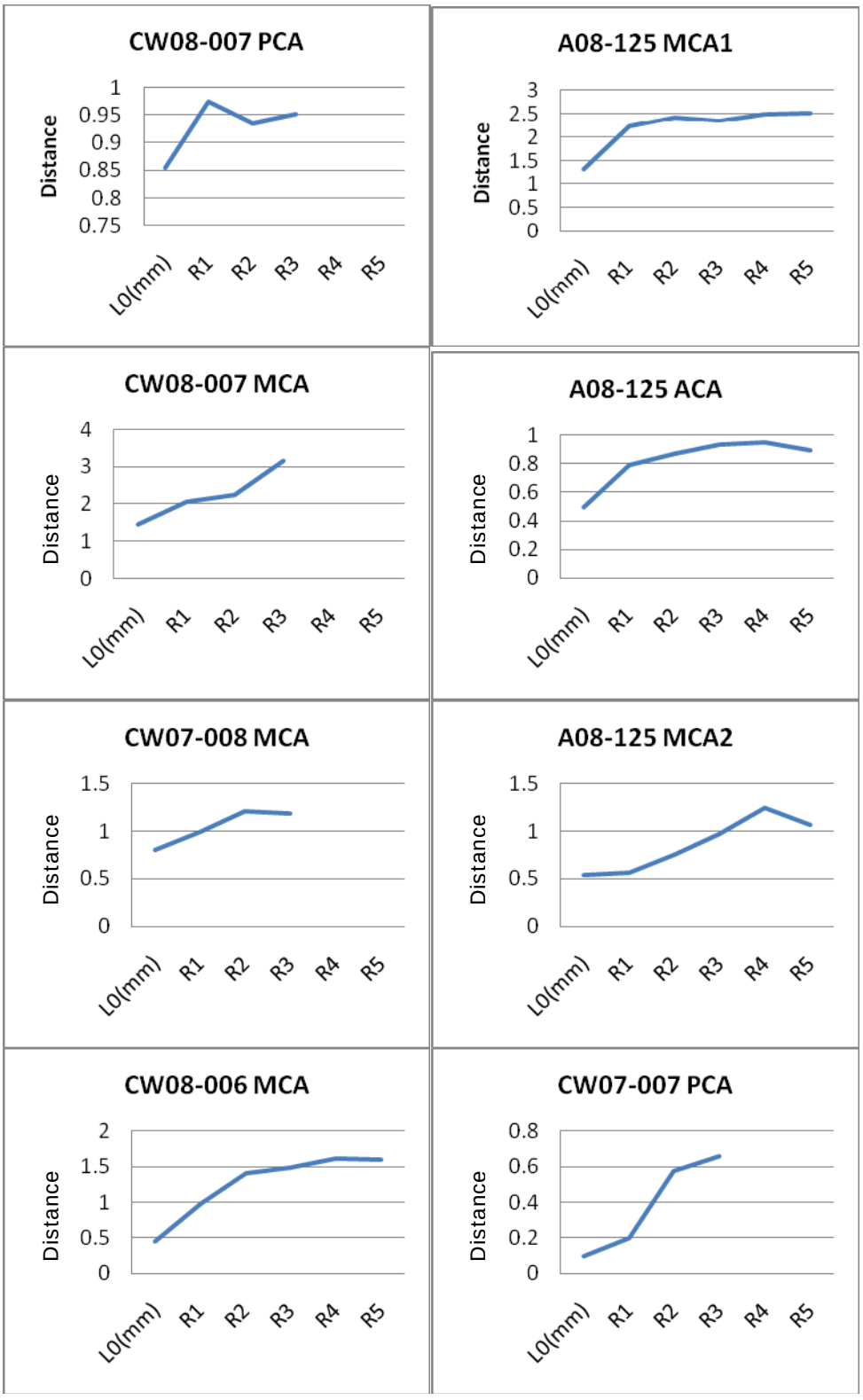

Figure 18: Graphical representation of unloaded state increasing with strain cycle. In some cases, five cycles were completed, and in others three cycles were completed. All dimensions are shown in mm.

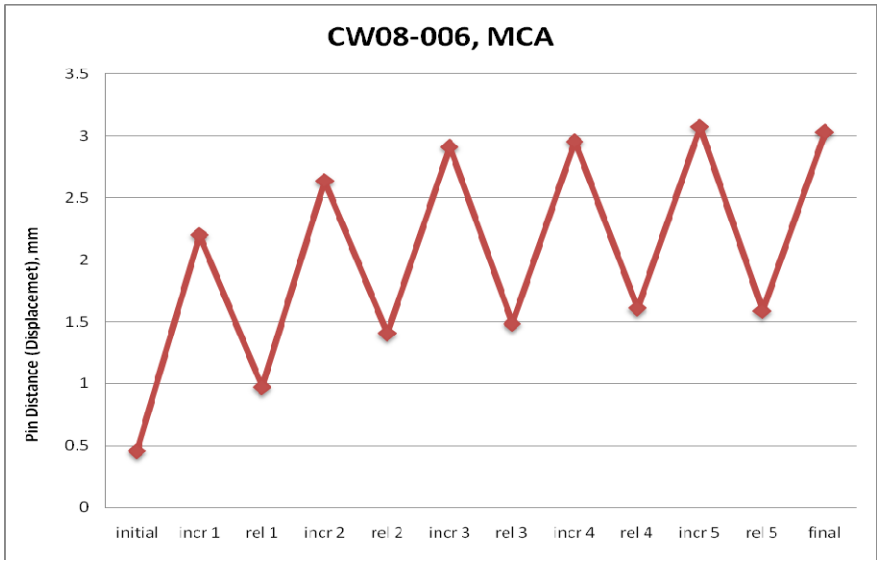

Figure 19: Graphical representation of one full experiment consisting of five loading and unloading cycles. At the end of the last loading cycle, the artery was stretched 564.82%.

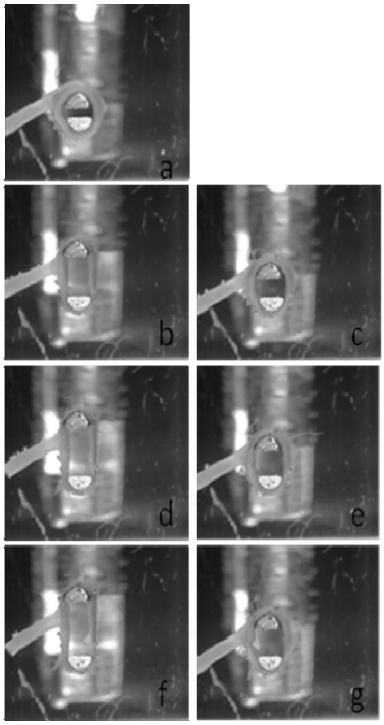

Figure 20: Camera images showing release and extend points. Image (a) corresponds to the initial load, (b) to the first increment extension, (c) to the first release and so on.

3.1.3 Histological Images and Tearing Mechanisms

In all of the previous experiments, a control artery segment was cut directly next to the tested portion and fixed in an unstrained state. Since the two segments are adjacent, it was assumed that the properties are similar, as long as there are no significant differences in arterial diameter or thickness and the origin of the sample was not near an arterial bifurcation or region of high curvature. In most cases, at strains under 200% no significant difference in damage between the control and stretched artery was found. It is expected for fenestrations to appear larger in the test case relative to the controls because of the folds in the IEL. Once these folds are stretched out and released, the fenestrations look larger and flatter. An example of this is shown in Figure 21.

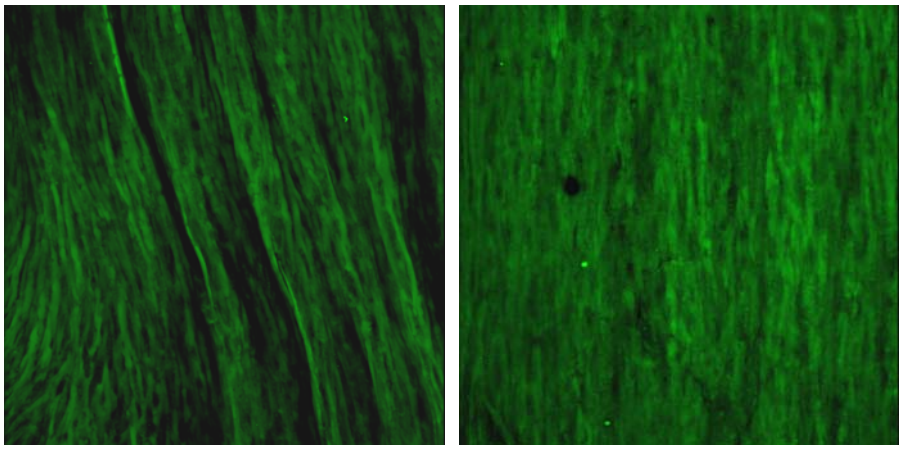

Figure 21: Left: 20x confocal image of CW07-008 MCA, unstretched segment. Right: 20x image of CW07-008 MCA, stretched to 171%.

In cases of high strains, such as with CW08-006 MCA, visible damage to the artery was seen even without a microscope. The damage occurred in multiple areas of the artery, and can be seen in Figure 22. In Figures23 and 24, the difference between normal and stretched

segments at 20x and 60x magnification are shown. In Figure 22, multiple tearing mechanisms can be seen. It seems as if the fenestrated sheet of elastin has completely ripped away from the bottom portion of the image, and that the artery has lost its overall directionality. This area also shows fibrous strands underneath the elastin. The difference in fenestrations in different layers of the arterial wall can be seen in Figure 25. This variation makes it difficult to quantify the fenestration area in a simple way.

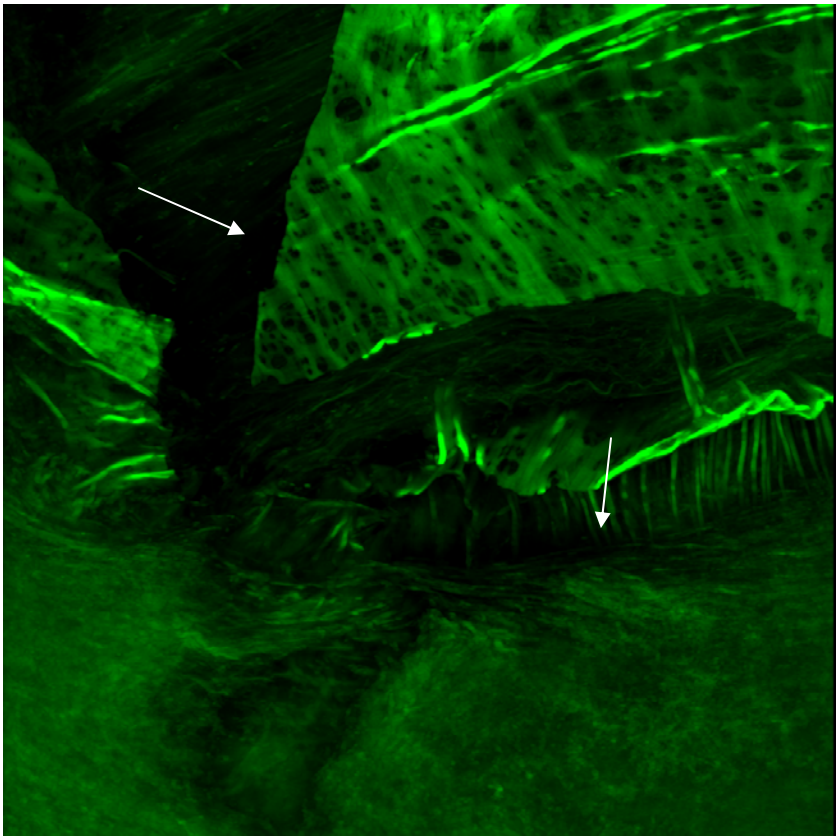

Figure 22: 20x confocal image of CW08-006 showing tearing and degradation of elastin, denoted by arrows.

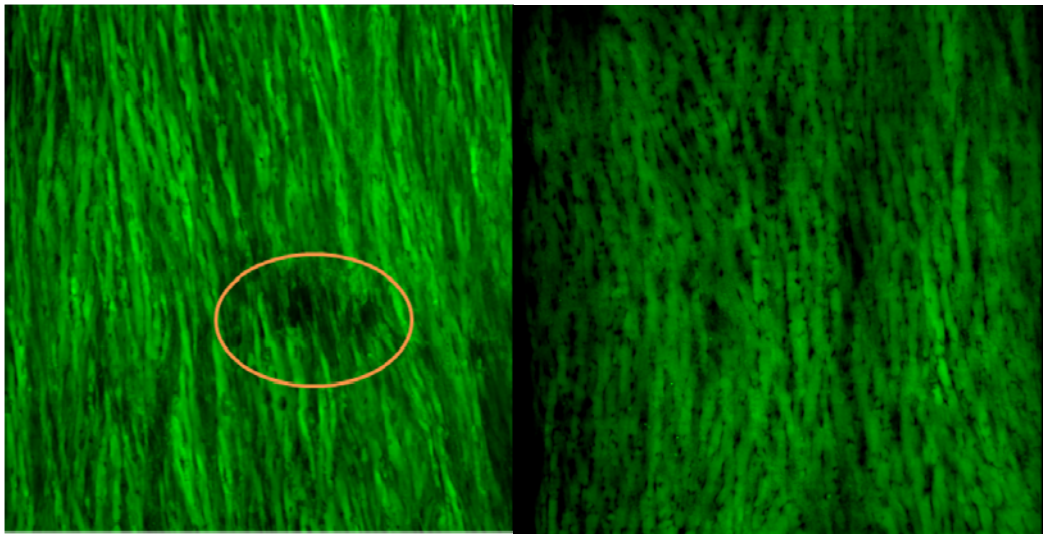

Figure 23: 20x confocal images of CW08-006 showing Left: unstretched segment, with possible weakened area highlighted, and Right: stretched segment, untorn area.

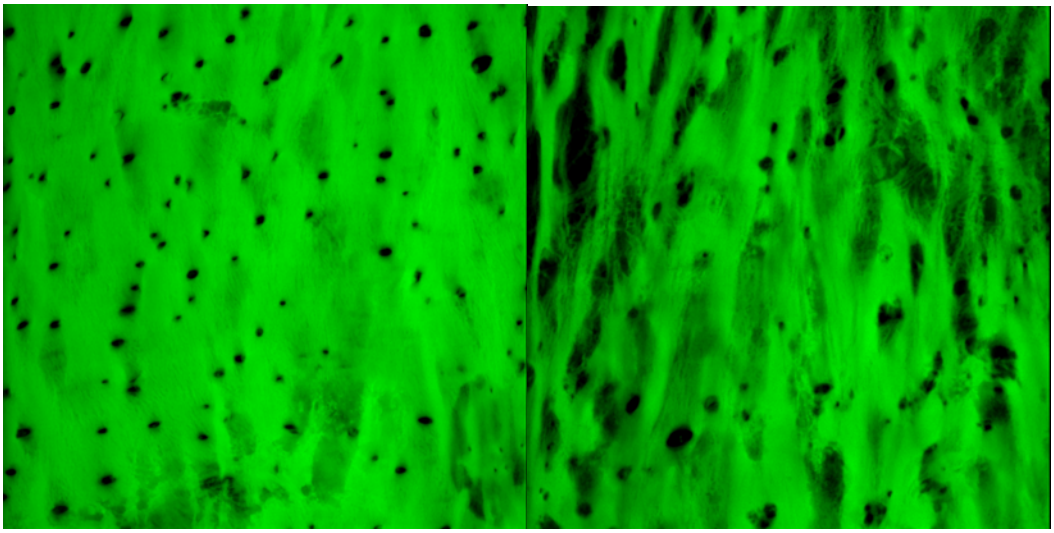

Figure 24: 60x confocal images of CW08-006 showing Left: unstretched segment, and Right: Stretched segment with enlarged fenestrations

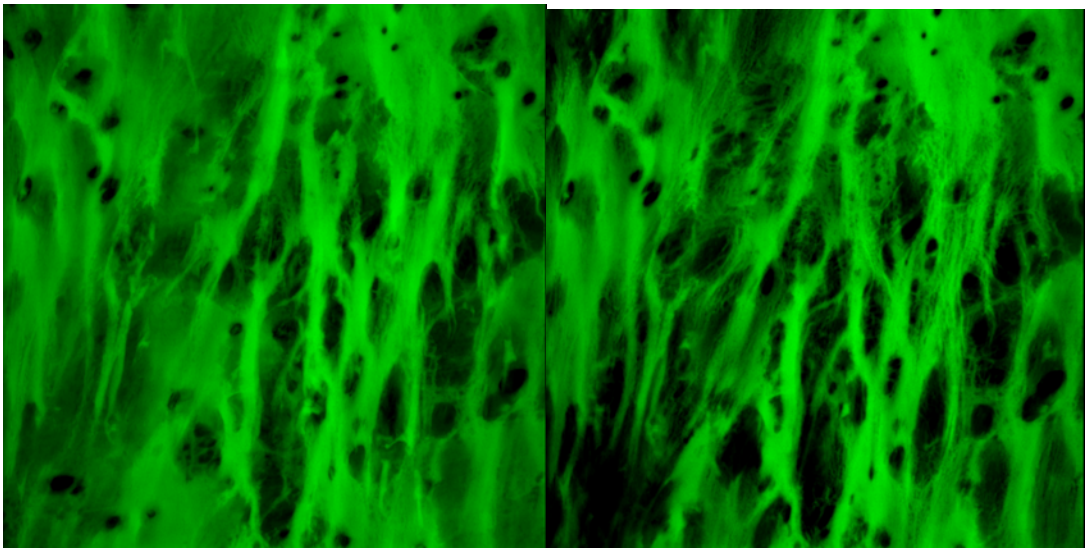

Figure 25: Stretched segments of CW08-006 MCA. Fenestration area differs in two images of the same location, but different depths. 60x magnification

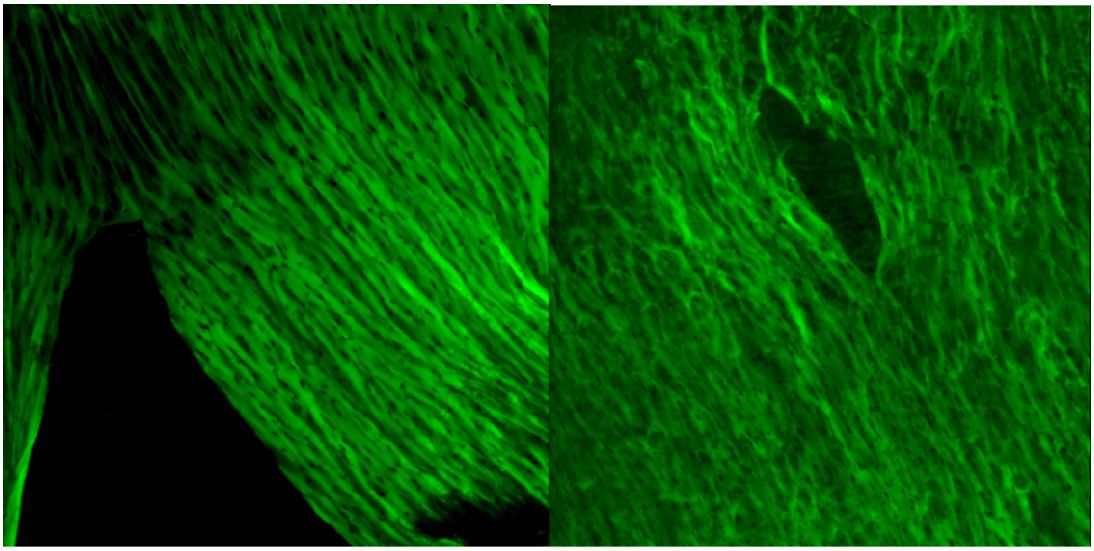

Figure 26: 20x Confocal Images of CW08-006 MCA, stretched segment

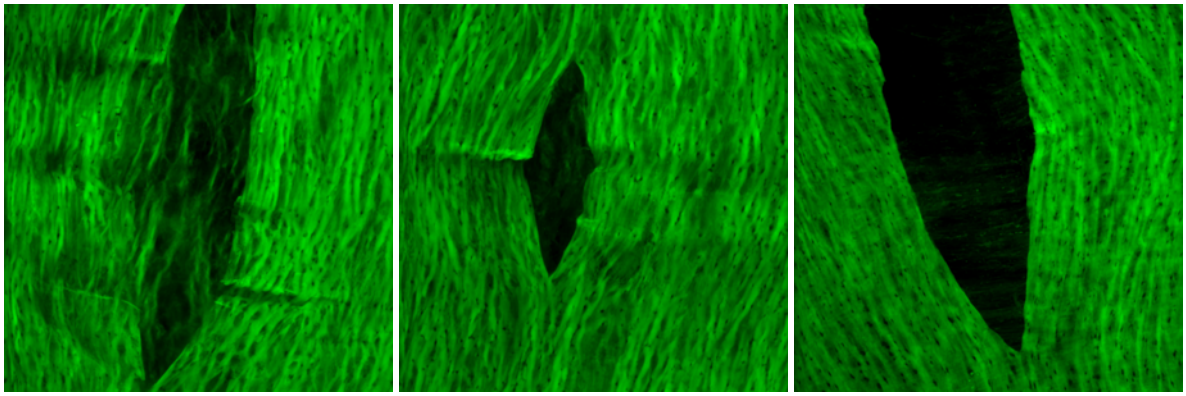

Figure 27: Confocal Images of Cat-Eye tearing mechanism. Left and Middle: Confocal Images of CW08-14, stretched to a load of 4.8N. Right: 20x Confocal image of A08-125 MCA2, stretched.

Tearing seems to occur parallel to the folds of the fenestration, tangent to the axial direction of the artery. These tears form a cat-eye shape as can be seen in the Figs. 26 and 26. We believe this mechanism is the main failure mode that arteries experience upon high circumferential strains. However, the cat-eye tearing mechanism was not the only failure mode seen in the arteries. In a few instances, tears were seen perpendicular to the grain of fenestrations and the axial direction, as shown in Figure 28. The evaluation of these tearing mechanisms may help in determining a visual state of damage that may not be evident in mechanical tests. The eventual use of this technology in conjunction with load measurement will help determine if there is a correlation between strain, load and tearing, and if so, where this point is. At this point in time, it is not known what level of damage is necessary to cause a measureable change in mechanical behavior.

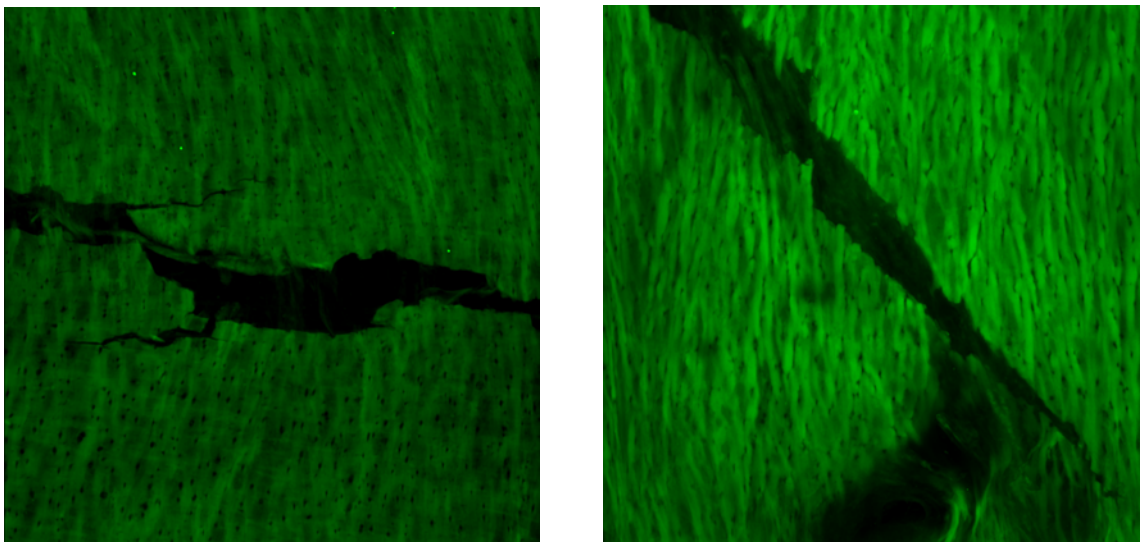

Figure 28: 20x confocal images of, Left: A08-125, unstretched, and Right: CW08-14 unstretched. Both arteries are MCA.

These tears, or cracks, vary in size and length, and are seen in both stretched arteries and control arteries. The control arteries have not been stretched circumferentially or loaded in any way. The source of these tears is not known at this time. It is possible that they occur naturally in healthy individuals, or are somehow associated with Alzheimer's disease or some other disease of the donor. Unfortunately, data of this kind is not available. Alternatively, these tears may arise during removal of the vessels from the brain or from other aspects of tissue handling such as during freezing/thawing or mounting the tissue on the glass slide. Significantly, cat-eye tears were never found in control samples, so we conjecture that cat-eye tears in the arterial wall results from high strain, Figure 29. The artery axis is shown with a dashed line. Left shows tearing under high strains, in the direction of the blue arrows. Right images shows cracking under unknown circumstances. Samples are mounted on the slide as shown in Figure 17

In order to better understand the source of the tears in the control group, we began an investigation of the effect of the freezing and thawing process on the mechanical and histological properties of the tissue. This work is described in the next chapter.

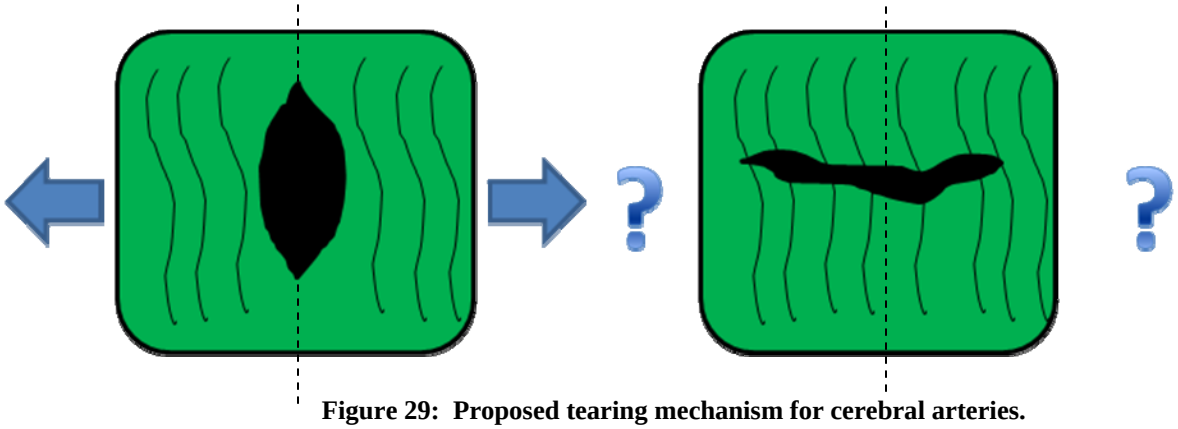

Figure 29: Proposed tearing mechanism for cerebral arteries.

3.1.4 Future histology work

In the future, it may be valuable to study the structure and orientation of the collagen fibers. When viewed under a confocal microscope, collagen does not autoflouresce naturally. Therefore, a stain must be used to view the collagen. Evaluation of collagen orientation will be useful for further development of constitutive models for the arterial wall.

Another improvement for the histology experiments would be the use of markers to designate specific areas of the artery. When artery segments are stretched, it is sometimes difficult to distinguish specific areas of interest. With the use of markers or a stain, the comparison of stretched and unstretched segments can be done more accurately.

4.0 INITIAL RESULTS AND DEVICE VALIDATION

To validate the device for use in uniaxial testing and perform an analysis of the freezing effects on arterial wall mechanics, several studies using fresh and frozen animal arteries have been performed. This chapter will discuss these studies as well as future work that is planned for the device.

4.1 FREEZING STUDY BACKGROUND AND PREVIOUS STUDIES

Because of the previously mentioned cracks in the control group of cerebral arteries we embarked on a study of the effect of the freezing and thawing process. Although it is not known if freezing is the cause of such cracks, this possibility provided a motivation for fundamental validation studies of the completed uniaxial device including load cell and motor. Before the freezing study began, background research was done on previous freezing studies of artery tissue. One study, performed by Venkatasubramanian et al. at the University of Minnesota, investigated the effects of freezing and cryopreservation on artery wall mechanics (Venkatasubramanian et al. 2005). Their techniques of freezing include cryoplasty and cryopreservation. Pig femoral arteries were frozen in a controlled rate freezer and weighed before and after freezing. Not only was the weight of the samples reduced after freezing, but the mechanical properties measured during uniaxial testing changed as well. The frozen samples

were stiffer than fresh arteries, and the unloaded circumference was larger. This last effect was not explained. The central conclusion of the study was that freezing impacted the mechanical properties of porcine femoral arteries. To confirm this result and explore its significance for our work, we performed several tests on fresh and frozen coronary arteries from cows and pigs using the uniaxial testing device. Animal arteries were chosen because fresh human arteries were not available.

4.1.1 Freezing Study Protocol

To test the freezing effects on the mechanical properties of arterial tissue and validate the device, the following protocol was designed. The final device, including the automatic motor control, load cell and modified pin mechanism, was used. A screen shot and description of the Labview interface is shown in Appendix A.

1. Circumflex or left anterior descending arteries are dissected from the heart of a cow or goat.
2. The artery is cut into ring segments of width 5mm to 8mm using small dissection scissors.. The number of sections depends on the total length of the artery. These sections are alternated fresh and frozen to provide the meaningful comparisons.
3. Samples are labeled using the following notation: Fresh samples are labeled with an Nx and frozen samples with Fx where x is the position number, Figure 30. The heart that the samples are taken from is labeled with a Cx or Gx for Cow or Goat heart, respectively. Each sample is labeled with the heart number and sample number. For example, in the fourth cow heart tested, the fourth fresh

sample is to be labeled C4-N4. For the analysis of the results, it is assumed that adjacent segments have similar mechanical properties and the arteries can be idealized as homogenous incompressible materials.

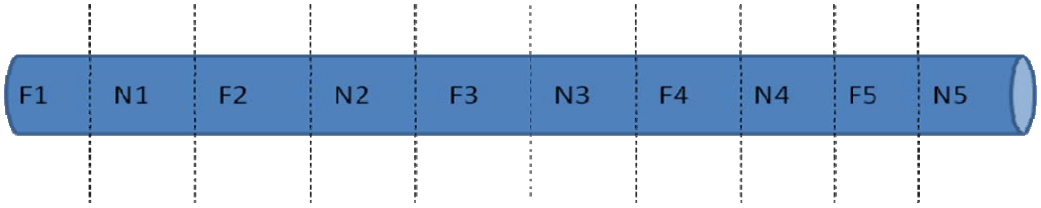

Figure 30: Diagram of example cutting order for freezing study.

4. Arteries chosen to be frozen are placed in Petri dishes and taken to the UPMC Brain Bank where they are frozen for 24 hours in the same freezer used to preserve the cerebral arteries. Fresh arteries are tested within 24 hours of slaughter, and refrigerated when not in use.
5. For frozen samples: Tissues samples are thawed for approximately 20 minutes at room temperature before testing.
6. The width of the segment is measured with calipers and recorded.
7. The ring segment to be tested is placed on the pins, which have been set to the "home" position on the device and immersed in the saline. This means the pins are touching, or experiencing small negative force. This position is identified as the zero position.
8. The artery is stretched to the point at which it experiences a load of 0.08N. This displacement associated with this load, called the contact point, was chosen because it seems to be the point at which most arteries appear "taut" on the pin mechanism.

9. At this point, the artery is dimensioned with the camera and NI-Vision software. Figure 30 shows a sample image from the camera at the contact point. For this study, strain calculations are based on changes in pin separation. Thickness measurements are made using six measured positions along the artery, Figure 31. Three are taken along the top pin and three along the bottom pin. These measurements are taken using the high definition camera, calibrated to convert pixels into millimeters. The thickness measurements are used later in the data analysis process to determine stress.

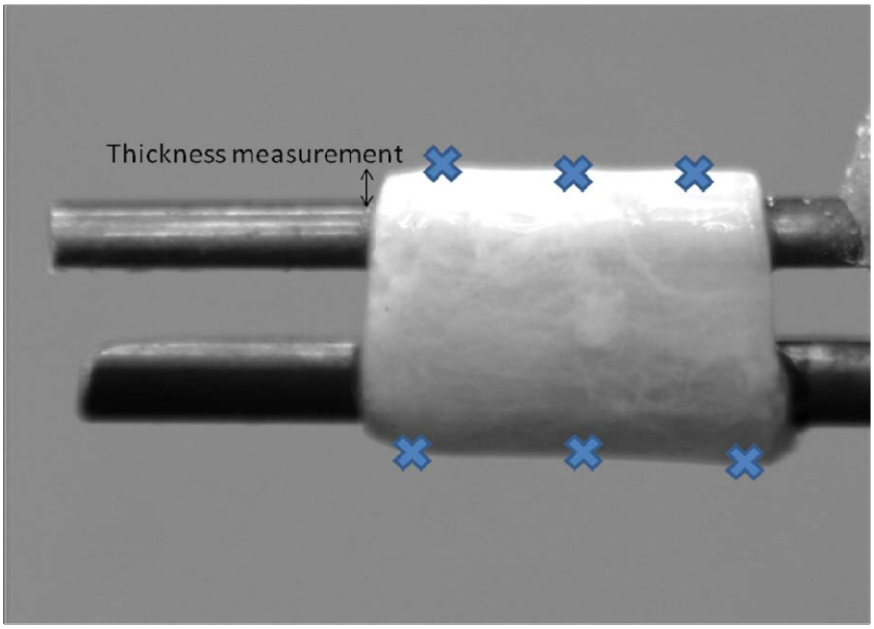

Figure 31: Photograph of thickness measurement protocol.

10. The artery segment is now placed in a cuvette of saline. The artery is preconditioned by loading the tissue to 1N for 6 cycles, each time retreating back to a position set by the operator. This position should be at a distance at least 1 mm less than the “contact point”. The device records data of load and

pin distance during this run. An example of preconditioning data can be seen in Figure 32.

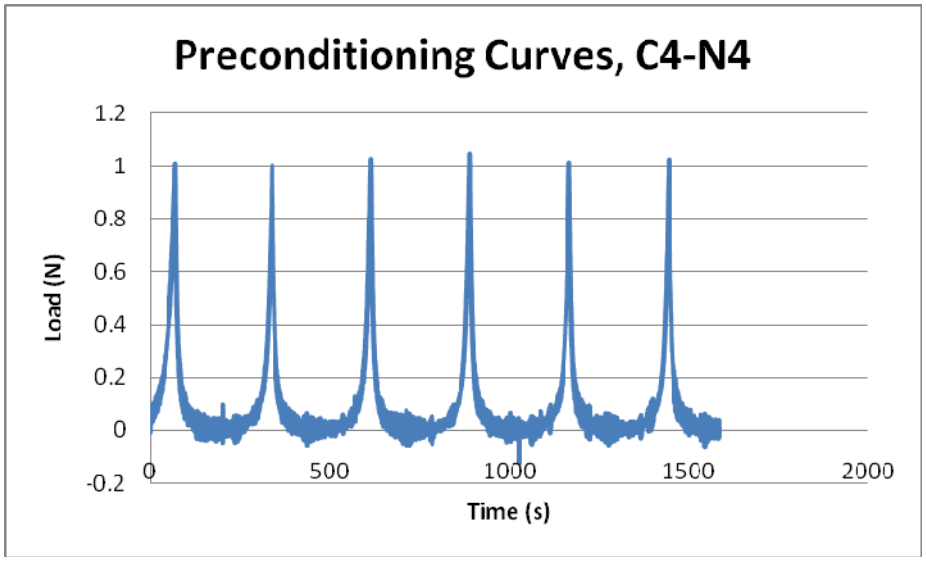

Figure 32: Preconditioning curves from sample C4-N4, shown Load vs. Time.

11. After preconditioning, the pins are retracted back to the home position, and the artery is then extended to the new contact point at 0.08N. In almost all cases, this new contact point is higher than the original before pre-conditioning.
12. A second test is run on the artery, loading it to 2N for 2 cycles, in the same manner as preconditioning.
13. Following this test, the device is retracted back to the home position and the artery is either discarded or put into a cuvette of saline for future testing.

4.1.2 Initial Freezing Study Results and Analysis

Several tests were run using the above protocol, in an effort to determine the relationship between fresh and frozen artery mechanics. The following protocol was used to determine a

stress-strain relationship from the data set for each sample. For this study, it is assumed that the sixth and final preconditioning curve contains the most consistent properties of the tissue.

1. Using loading curve 6, collect all data from increasing load and strain.
2. From the thickness values measured, take the average of the minimum thickness of each sample to use as a universal thickness for the study.
3. Calculate Stress for each load point. Stress is calculated assuming the force on each side of the tissue is equal, as shown in Figure 33 and Figure 34. In addition, the material is idealized as incompressible and homogeneous with constant thickness and width. Eq. 3 is used to calculate stress.

   Stress = F(N)/(2* (width of segment * thickness)). (3)
4. Calculate L0. To determine the most appropriate value for L0, a stress value is first chosen (typically 0.01 to 0.03 N/mm^2). Filter stress values to reduce noise from load cell, using a low-pass filtering method, as performed with steps 5 through 9.
5. Beginning with the fifth stress value, take the average the four previous points and itself. Repeat this process for each sequential data point.
6. Repeat the entire process on the averaged data for a twice-averaged value of stress.
7. From the twice-averaged stress, find the point at which stress equals the desired value from step a. This point is the starting point for the data set, and L0 is set as the distance between the pins at this stress value.
8. Strain is determined from Eq. 2, and L0 should have a strain of 0. This data is then plotted against the original, un-averaged stress values starting from L0.

9. Compare all samples on the same graph

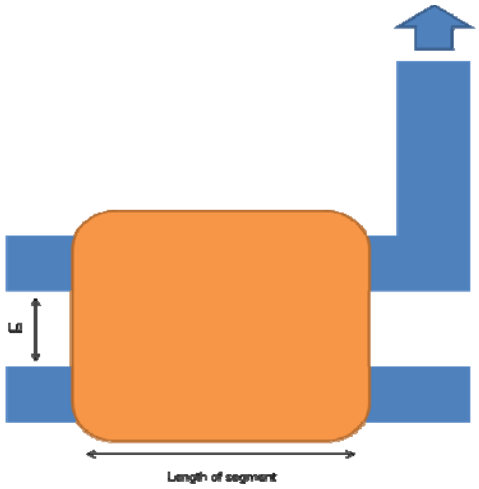

Figure 33: Diagram of length and Lo dimensions

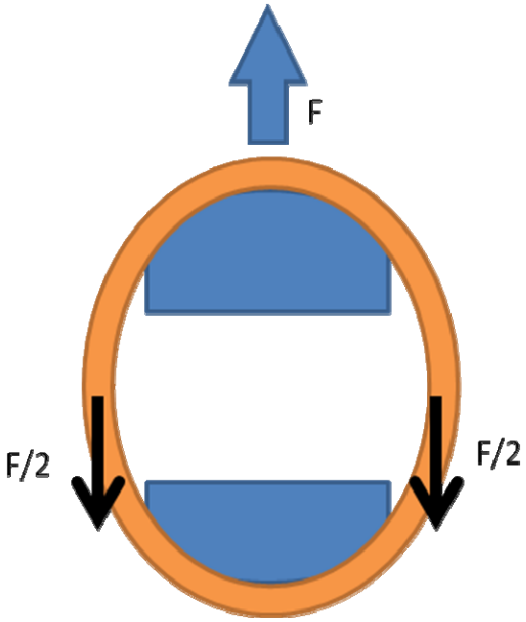

Figure 34: Diagram of force distribution within artery sample

Figure 36 and Figure 37 show graphs for all samples. Both sample sets used an L0 starting stresss of 0.03N/mm2. The differences in these values may be why the two sample sets differ in stress and strain range. For C3, the thickness value used was 0.39mm. For C4, the thickness value used was 0.2mm.

C3 was cut according to Figure 29, to directly compare stress-strain curves from adjacent segments of fresh and frozen tissue. C4 was cut according to Figure 35, to better compare adjacent fresh arteries with fresh arteries as well as with adjacent frozen arteries and vis versa.

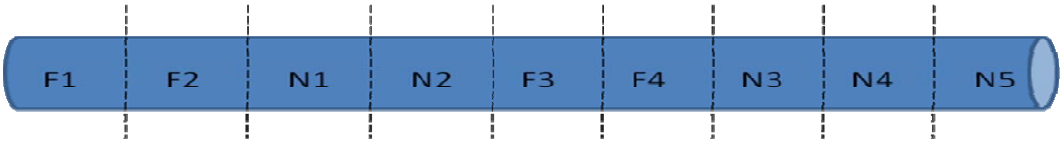

Figure 35: Schematic of C3 artery cutting method.

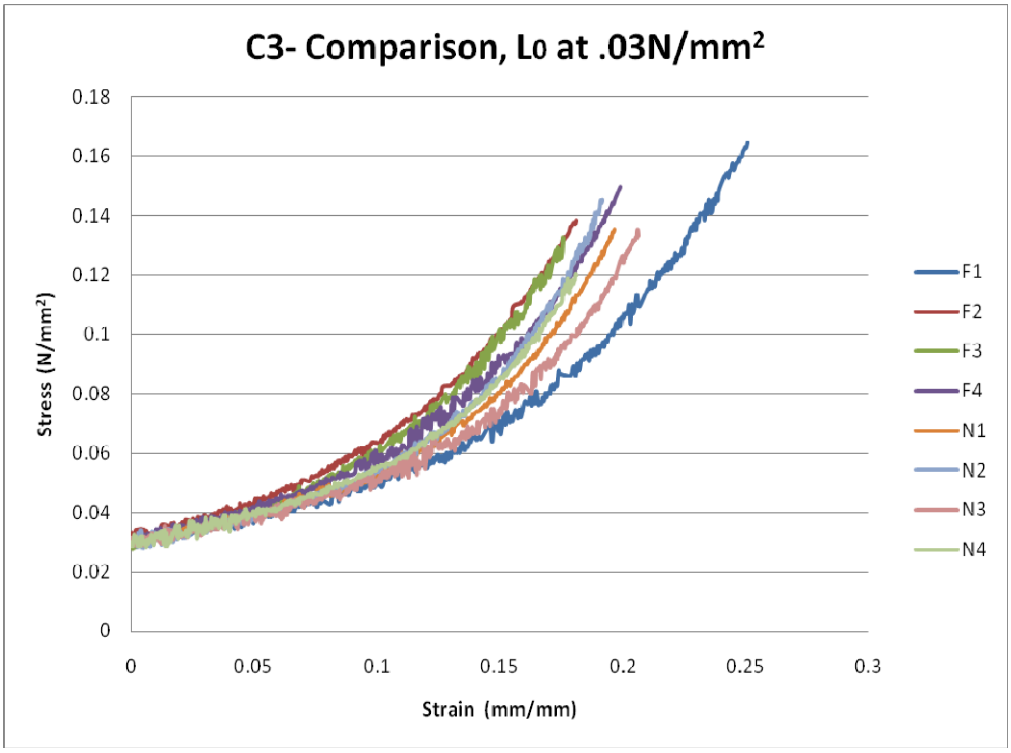

Figure 36: Stress-strain curves for Cow heart 3 (C3). From Left: F2, F3, N2, F4, N4, N1, N3, F1

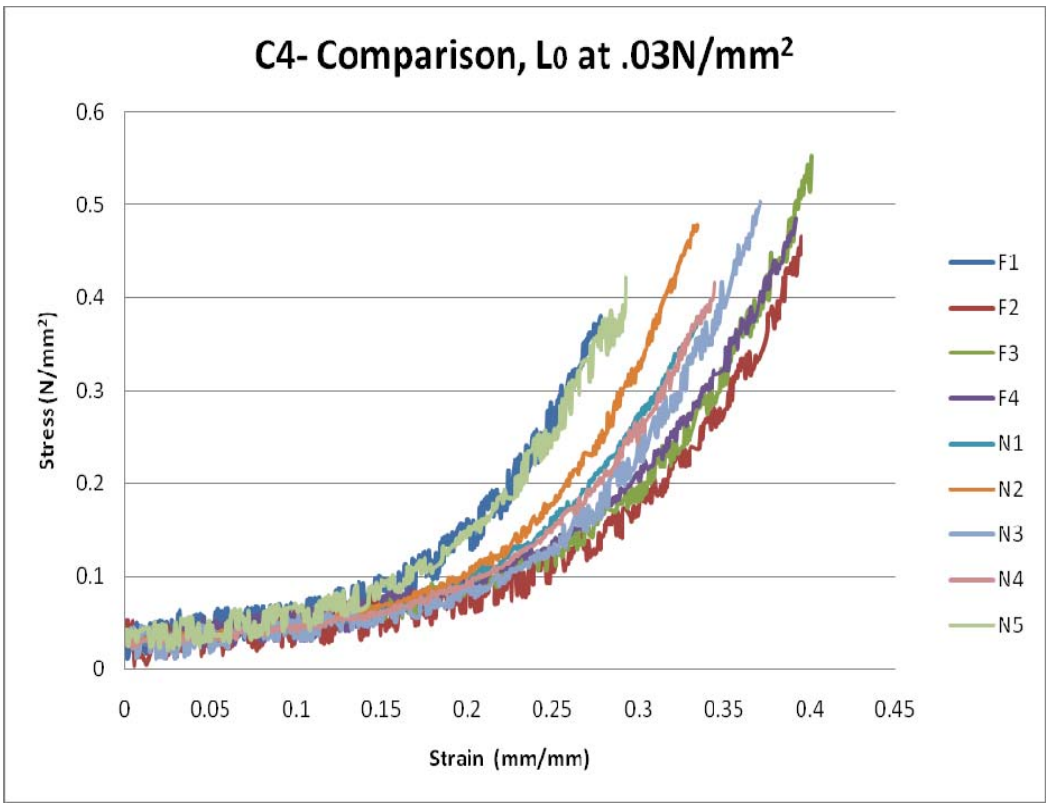

Figure 37: Stress-strain curves for Cow Heart 4 (C4). From Left: F1, F3, N2, N1, N4, N3, F4, F3, F2

The two graphs show the stiffness of all artery segments increases with strain level. Although the general shape of the graph is the same for each sample, at high strains, the segments seem to differ greatly. The graphs also do not show a correlation between fresh and frozen samples, or sample order. This issue presents a need to normalize the stress-strain curves for more accurate comparison. Although the analysis method currently attempts to standardize stress with the filtration method, a normalization method would be helpful in the comparison of several data sets and eventually lead to a modified protocol.

Furthermore, a study was performed on only fresh arteries to determine if the mechanical properties of adjacent segments are similar. The results were inconclusive as to whether the properties were significantly similar or different. This study is shown in Appendix B.

To verify the device is consistent and repeatable, a sample was tested twice on the device at two different time points. The sample, a fresh segment of tissue, was tested once, following the testing protocol, and then again following a twelve hour gap of time. The sample was removed from the system and placed in a cuvette of saline between the two tests. The graph is shown in Figure 38, and indicates a very high level of repeatability.

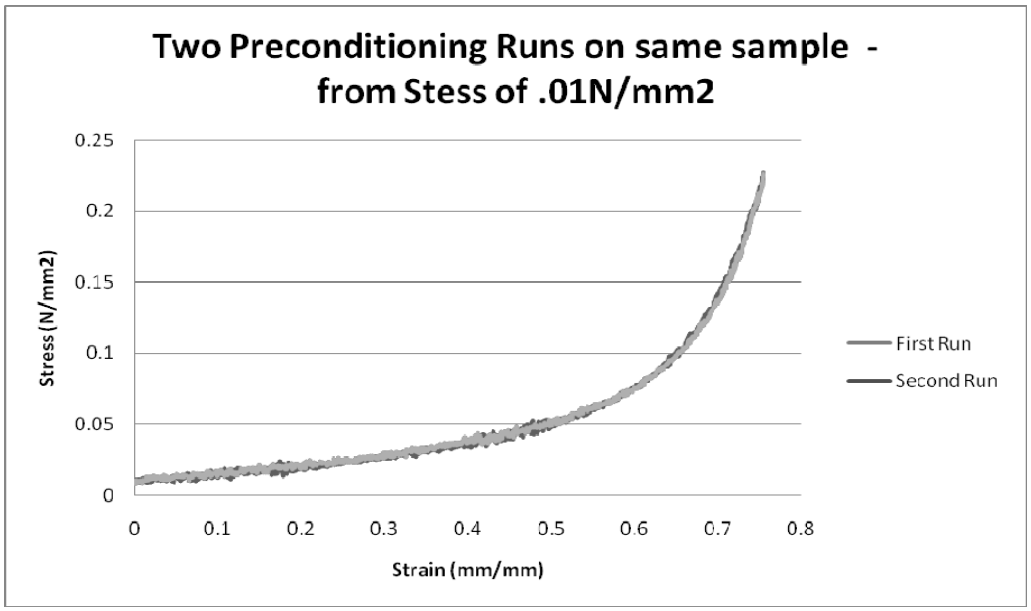

Figure 38: Validation test showing consistency of device and sample behavior.

At this point in time, we do not attempt to form conclusions as to whether freezing affects the mechanical properties of arteries. This will be addressed in a future work, once the source of inter-specimen variability for adjacent segments is resolved. These preliminary results lay the foundation for future studies in which a statistical analysis will be performed to evaluate the significance of freezing on the mechanical properties of the tissue.

Several issues remain to be addressed. The best method for determining L_0 remains an open question. The loading curves are highly influenced by this choice, yet it is difficult to measure due to the flat toe region at low loads, as shown in Figure 39. This graph shows load vs.

displacement of the pins during a cycle in preconditioning. The large toe region is evident, making it very difficult to determine the appropriate point to designate as L_0. The stress filtering method was used to standardize a determination method for L_0 for comparison purposes. The difficulty determining L_0 will be an issue to be explored in the future.

Another challenging question is how to handle variations in thickness along the length of the artery. Since the intramural stress is calculated by dividing the total load by the cross sectional area, these variations can influence the results for stress distribution. If the material was truly homogeneous, this thickness would have a clear meaning. However, the wall content of the main load bearing components (elastin and collagen) can be the same in two ring segments while the wall thickness varies greatly due to the unequal distribution of materials with insignificant contribution to load bearing. For example, localized fat distribution or plaque build can change the wall thicknesses by more than 25 % without contributing significantly to load bearing.

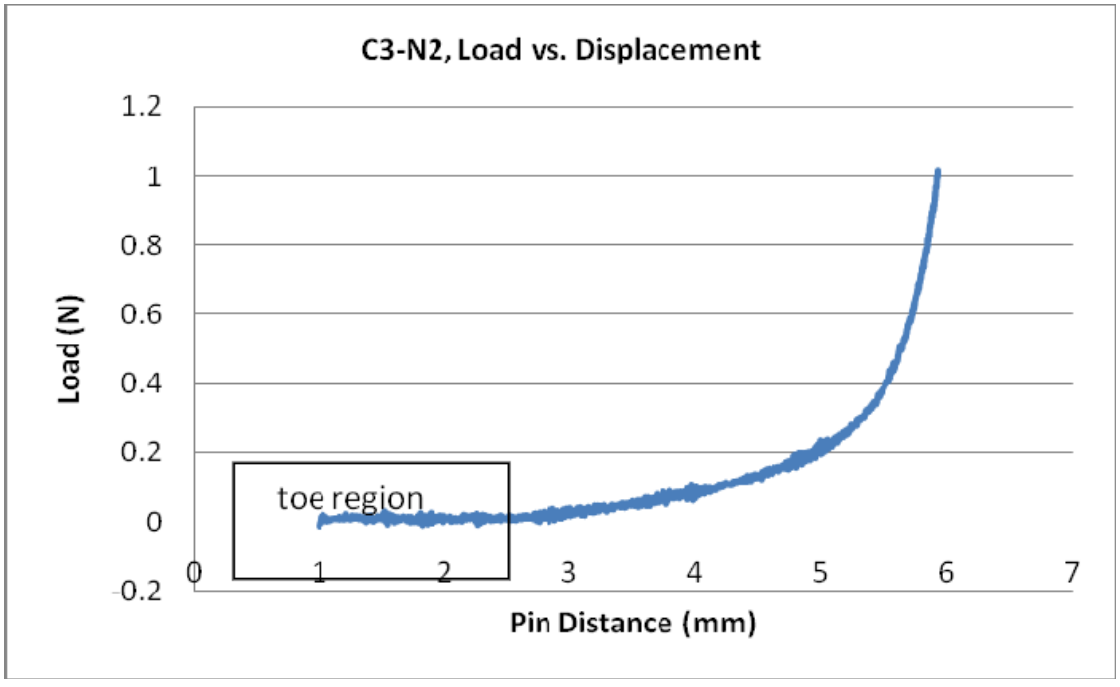

Figure 39: Load vs. Displacement curve for C3-N2

Another issue is the method of strain measurement. In these preliminary studies, the strain is approximated using the change in pin to pin distance. This is not expected to be reliable at larger strains due to the increased significance of the inhomogeneity of the strain field. We are now using an updated protocol in which strain is calculated from measurements of the displacement of markers placed on the tissue (away from the pins). These markers are viewed using the camera, which takes snapshots of the segment at increments during the test. This approach is also expected to provide a more reliable estimate of the value of L_0. A relatively minor issue is the tendency of the ink markers to diffuse. Currently, this is not a problem. However, it may be necessary to decrease the distance between markers to lessen end effects. In this case, it may be necessary to investigate new marker methods or materials.

An additional issue in the uniaxial stretching protocol is the timing between tests. Currently, the time between preconditioning and testing is not recorded. This time is typically one to five minutes, because the test is run almost immediately after the preconditioning cycles. We have not explored the significance of this choice.

For simplicity, these preliminary studies were conducted at room temperature. It is expected that the material response will be somewhat temperature dependent. In the future, the tests can be performed at physiological temperatures using a temperature bath. It is also possible that the mechanical properties of the artery will be affected by the particular choice of freezing and thawing protocols. These issues will possibly be considered in the future.

Artery walls are anisotropic, largely due to the collagen fiber orientation. Therefore, it is important that each ring be cut with a known orientation to the main axis. In addition, in cases where it is desired that the ring segments have similar properties, care should be taken to avoid

regions such as highly curved segments and bifurcations where this orientation is expected to vary with position. A ring cutter was previously designed for related work. This device was capable of cutting multiple ring segments with consistent thickness and orientation. However, it was designed for opening angle experiments with much thinner rings. In the future, this cutter will be adapted for thicker ring segments.

5.0 CONCLUSION

A device to uniaxially stretch arterial ring segments has been successfully designed and built. It is capable of accurately measuring applied load and displacement and can be used to fix tissue at both prescribed loads and strains for later histological evaluation. The uniaxial system was used to obtain preliminary data on the failure mechanism of the internal elastic lamina, IEL, of cerebral arteries under large strains. Initial data was obtained comparing the stress/strain response of fresh and frozen tissue. Several issues remain to be resolved. The most significant are related to accurate determination of the unloaded length and more localized measurements of strain. Significant steps have already been made to resolve these issues. Further understanding the failure mode of the IEL and determination of mechanical parameters associated with cerebral arteries under high strains will contribute to the aforementioned constitutive equations and ultimately the field of arterial mechanics.

APPENDIX A

LABVIEW SCREENSHOT

Figure 40 shows a screenshot of the Labview program used in the uniaxial testing protocols. The "home" position, section **a**, is set when the pins are touching, creating a small negative load. This position is set before testing. The "contact" position is set when the load on the artery is 0.08N, as shown in section **b** of the screenshot. Finally, to begin preconditioning or a test, section **c** is used to program load-controlled parameters such as number of cycles and maximum load. This section is also used to program the minimum position the device will reach during the unloading curve of a cycle. This position is set to a distance at which the user knows the artery will not experience a load. For very large arteries this distance can be larger to save experiment time. Section **d** of the figure shows two display panels for position and load with respect to time.

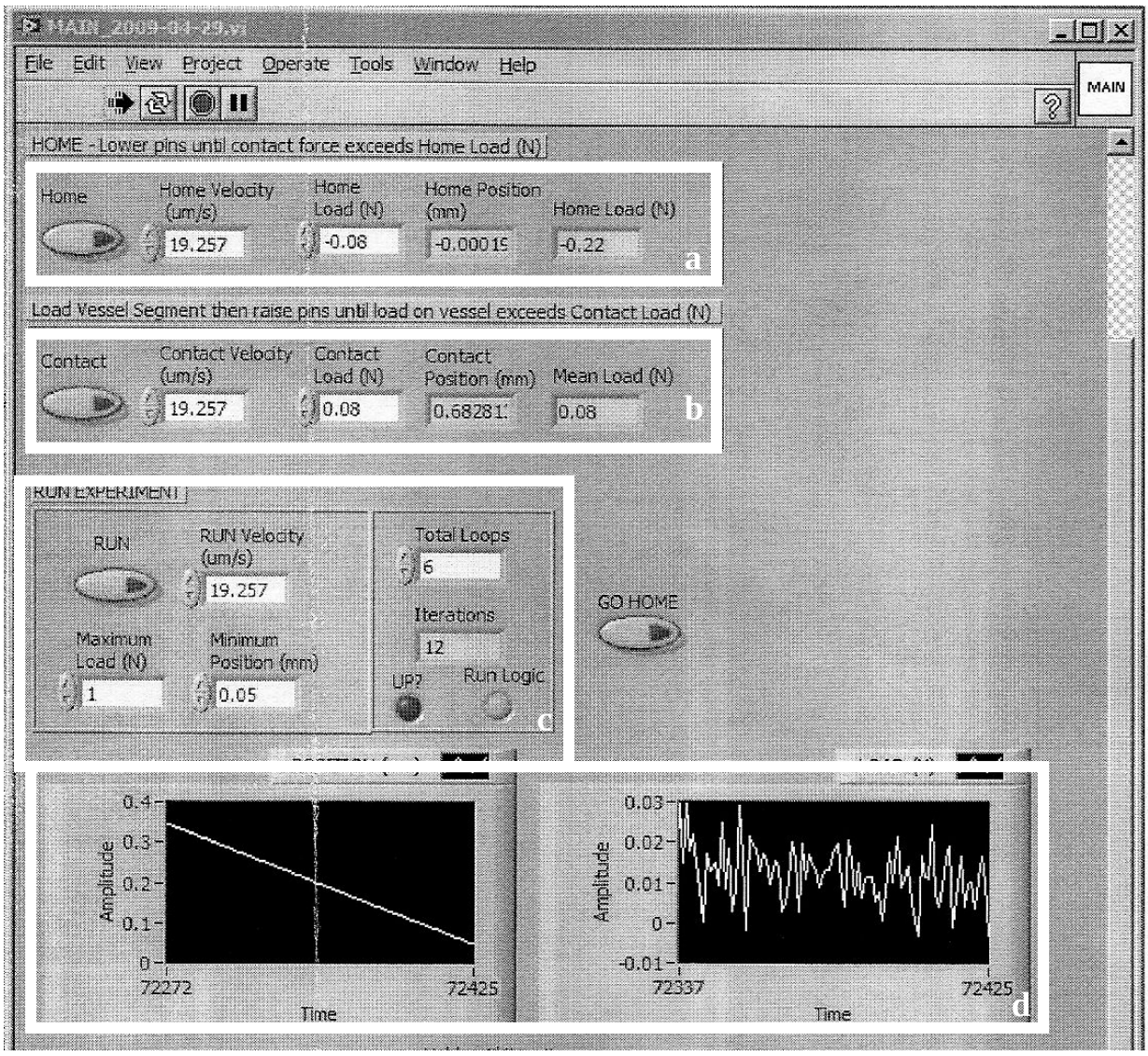

Figure 40: Screen shot of Labview program used to run uniaxial tests.

APPENDIX B

ADDITIONAL STUDY

An additional study was performed to determine if the stress-strain relationship is similar between adjacent segments of an unfrozen arterial segment. The protocol from Chapter 4.0 was used for a fresh circumflex bovine artery. The results from this study were analyzed in the same manner as the freezing protocols, and are shown in Figure 41. This data shows that adjacent segments treated in the same fashion are not consistent in their mechanical responses.

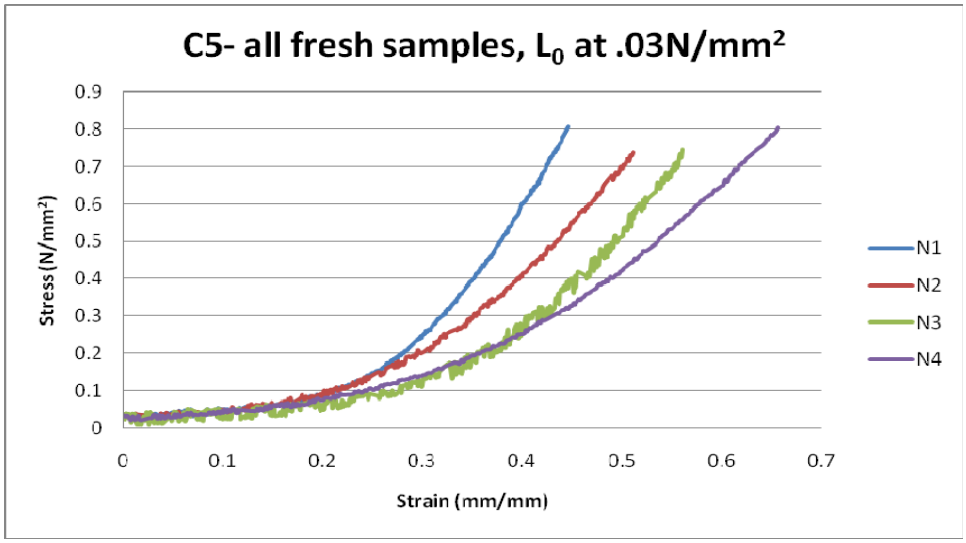

Figure 41: Fresh artery study, showing curves for four adjacent segments. N1, N2, N3, N4.

BIBLIOGRAPHY

References:

Allcock JM, Canham PB. *Angiographic study of the growth of intracranial aneurysms.* **J Neurosurg 45:**617–621, 1976

Barry, J., Hydrean, C., Young, B. *Device used for stretching and fixing cerebral artery tissue in preparation for imaging.* Senior Design Project Report, **University of Pittsburgh**, 2007.

Campbell, G. J., Roach, M.R. *A Physical Model for the Formation of Evaginations: A Prospective Precursor to the Creation of Saccular Aneurysms.* **Stroke** Vol. 15, No. 4, 1984

Canton, G., Levy, D.I., Lasheras, J.C. *Hemodynamic changes due to stent placement in bifurcating intracranial aneurysms.* **J Neurosurg 103:** 146-155, 2005.

Gao, L., Hoi, Y., Swartz, D.D., Kolega, J., Siddiqui, A., Meng, H. *Nascent aneurysm formation at the basilar terminus induced by hemodynamics.* **Stroke,** 39(7), pp 2085-2090, 2008.

Gonzalez, J., Briones, A., Starcher, B., Conde, V., Somoza, B., Daly, C., Vila, E., McGrath, I, Gonzalez, M., Arribas, S. *Influence of elastin on rat small artery mechanical properties.* **J. Exper. Phys.** 90, 463-468, 2005.

Hassler, O. Morphological *studies on the large cerebral arteries with reference to the aetiology of subarachnoid hemmorage.* **Acta Psychiat. Neurol. Scand.** 36**,** Suppl. 154, 1961

Kaymbe, K. N. T., Sasahara, M., Hazama, F. Cerebral Aneurysms and Variations in the Circle of Willis. **Stroke** Vol. 15, No. 5, 846-850, 1984.

Li, D., Robertson, A.M. (a). *A Structural Multi-Mechanism Constitutive Equation for Cerebral Arterial Tissue,* **International Journal of Solids and Structures,** 46(14-15), pp. 2920-2928. doi:10.1016/j.ijsolstr.2009.03.017, 2009.

Li, D., Robertson, A.M. (b). *A Structural Multi-Mechanism Damage Model for Cerebral Arterial Tissue,* **Journal of Biomechanical Engineering,** (in press, 2009)

Li, D., Robertson, A.M. (c). *Finite Element Modeling of Cerebral Angioplasty using a Multi-Mechanism Structural Damage Model Student Paper Competition,* **ASME 2009 Summer Bioengineering Conference,** June 17 -21, 2009, Lake Tahoe, CA.

Meng, H., Wang, Z., Hoi, Y., Gao, L., Metaxa, E., Swartz, D. D., and Kolega, J. *"Complex Hemodynamics at the Apex of an Arterial Bifurcation Induces Vascular Remodeling Resembling Cerebral Aneurysm Initiation,"* ***Stroke***, 38(6), pp. 1924-1931, 2007.

Morimoto, M., Miyamoto, S., Mizoguchi, A., Kume, N., Kita T., Hashimoto, N. *Mouse model of cerebral aneurysm: experimental induction by renal hypertension and local hemodynamic changes.* **Stroke: A Journal of Cerebral Circulation,** 33(7), pp. 1911-1915, 2002.

Nystrom, S.H.M. *Development of intracranial aneurysms as revealed by electron microscopy.* **J. Neurosurg.** 20, 329-337, 1963

Scott, S., Ferguson, G.G., Roach, M.R. *Comparison of the Elastic Properties of Human Intracranial Arteries and Aneurysms.* **Canadian Journal of Physiology and Pharmacology,** Vol 50, 1972.

Taren, James A, *"Aneurysm."* **American Journal of Nursing***:* Volume 65, No. 4, p. 88, 1965.

Toth, B.K., Bojtar, I., Raffai, G. Biomechanical properties and analysis of the mechanical parameters of human cerebral aneurysms. **Biomechanics**, 2006/3.

Venkatasubramanian, R.T., Grassl, E.D., Barocas, V.H., Lafontaine, D., Bischof, J.C. Effects of Freezing and Cryopreservation on the Mechanical Properties of Arteries. Annals **of Biomedical Engineering**, vol. 34, No. 5, 823-832, 2006.

Wulandana, R., Robertson, A.M. *An Inelastic Multi-Mechanism Constitutive Equation for Cerebral Arterial Tissue*. **Biomechanics and Modeling in Mechanobiology**, 4(4), p 235-248, 2005.

Image References:

Aneurysm in the Brain. MD Consult. www.mdconsult.com/das/patient/body/142368474-2/0/10041/35264.html

Maastricht. November 2005. Stijin A. I. Ghesquiere. www.applesail.net